2022-01-03

Biodegradable Cryogels for Adsorption and Electrochemical Oxidation of Organic Dyes

Abuhatab, Saqr S

UNIVERSITY OF CALGARY

Biodegradable Cryogels for Adsorption and Electrochemical Oxidation of Organic Dyes

by

Saqr Sufian Abuhatab

A THESIS

SUBMITTED TO THE FACULTY OF GRADUATE STUDIES

IN PARTIAL FULFILMENT OF THE REQUIREMENTS FOR THE

DEGREE OF MASTER OF SCIENCE

GRADUATE PROGRAM IN CHEMICAL ENGINEERING

CALGARY, ALBERTA

JANUARY, 2022

Abstract

The supply of clean water is becoming one of the greatest challenges of the 21st century. Therefore, sustainable and cost-effective measures must be developed and implemented to reduce water scarcity and prevent contamination of our water systems. This work aims to develop novel, environmentally-friendly 3D structured adsorbents for the removal of dissolved organic pollutants from wastewater. This was achieved by developing hydrophobic cryogels composed of TEMPO-oxidized cellulose nanofibers (TOCN) and electrochemically exfoliated graphene (EEG). TOCN/EEG cryogels were hydrophobized by incorporating oleic acid (OA) into the precursor gels. The cryogels were synthesized by mixing the components at 50 °C and 300 rpm for one hour, followed by freeze-drying the gels. The effect of OA loading, TOCN/EEG weight ratios (1:1 and 1:2), and initial solids content were systematically investigated through microstructural and rheological characterization of the precursor gels, and the morphology and adsorption capacity of the derived cryogels.

The optimum OA loading for the hydrophobization of TOCN (HTOCN) was found to be 5 wt.%, at which the strongest gel was obtained. The initial solids content and EEG loadings in the precursor gel alter the morphology and adsorption capacity of the derived cryogels. The maximum adsorption uptake was increased by 180% for the 1:1 HTOCN/EEG weight ratio when the initial solids content in the precursor gels was increased from 1 wt.% to 4 wt.% compared to only 70% rise when the solids content was increased from 1.5 wt.% to 6 wt.% for the 1:2 HTOCN/EEG cryogels. The drop in the adsorption capacity enhancement of the 1:2 HTOOCN/EEG cryogels was attributed to the higher extent of EEG sheets aggregation at higher EEG contents. The electrochemical regeneration studies confirmed the ability to oxidize the methylene blue adsorbed onto the cryogels with minimal changes in the cryogels' adsorption capacities after multiple

regeneration cycles. The cryogel made of 1:1 HTOCN/EEG with 1 wt.% solids content gel was tested for 18 adsorption-electrochemical regeneration cycles with no observable mass loss and retained adsorption capacity confirming the feasibility of the proposed approach for developing adsorbents with long-term stability.

Dedication

I dedicate my dissertation work to the most important people in my life

To my parents: ***"Sufian and Rania"***

To my sisters ***"Reham, Reema, and Raghad"***

To my brothers ***"Abedalqader, Osama, and Qusai"***

Thank you for your unconditional love and endless support! I love you and I would not be here today without your support!

Acknowledgment

I would like to express my sincere gratitude to my supervisor, Dr. Milana Trifkovic, who truly inspired me in many different ways, for her continuous support, patience, motivation, supervision, and immense knowledge. I would also like to thank Dr. Edward (Ted) Roberts for his encouragement, guidance, insightful comments and questions, and co-supervising my internship.

I am so grateful to Omar Saleh, the CEO of Recycl3D Inc., and Mitacs for giving me a great internship opportunity and financially supporting this project; the funding and internship opportunity through Mitacs Accelerate Research Internship Program are greatly appreciated.

A special thanks to our research group members at the University of Calgary for their feedback and support, especially Aleksandra Govedarica, for sharing her knowledge, the valuable discussions, and the laser scanning confocal microscopy training. I would also like to thank Rajas Shah for training me on different rheological characterization techniques and sharing his valuable knowledge.

My deepest thanks to my close and supportive friends, especially Nedal Marei, for his unwavering support, inspiration, and helpful advice and suggestions. Thank you for the truckloads of good times and for being such a great friend – You are awesome!!

Table of contents

List of figures

List of figures in supporting information

List of tables

Chapter 1

Introduction

1.1 Background

Clean water is essential for sustaining human health, agriculture, economic development, and the whole ecosystem. The global water crisis, shortage of freshwater, contamination of water, and increasing volumes of wastewater are threatening to further damage the ecosystems. Larger effluents of wastewater are generated due to the growing water usage, and where these are not sufficiently treated, freshwater bodies are continuously threatened. Therefore, and due to the environmental concerns instigated by wastewater, more effort is being dedicated to establishing new, cost-effective, and sustainable technologies for wastewater treatment (Rashid et al., 2021).

To date, various wastewater treatment technologies have been developed to minimize wastewater discharges and mitigate pollutants, classified into physical, chemical, and biological treatment methods (Musa and Idrus, 2021, Ma et al., 2021). The physical methods include sedimentation, membrane filtration, and physical adsorption (Mustafa and Asmatulu, 2020, Hu and Xu, 2020). Biological treatments such as activated sludge and biofilm are the most used biological techniques for water treatment (Samer, 2015, Mustafa and Asmatulu, 2020), while oxidation, coagulation, flocculation, chemical adsorption, and ozonation are widely used chemical treatment methods (Hu and Xu, 2020, Elshorbagy and Chowdhury, 2013, Lofrano et al., 2013).

Among the various available treatment techniques, adsorption is a highly effective, simple, and economical process for the removal of contaminants from water (Renu et al., 2016, Doke and Khan, 2013). The important characteristics of an adsorbent include large surface area,

reproducibility of adsorbent synthesis, low cost, high adsorption capacity, fast adsorption rate, selectivity, and the ability to be regenerated (De Gisi et al., 2016, Pietrzyk and Frank, 1979). The adsorption process is divided into physical and chemical adsorption based on adsorption forces between the adsorbate and adsorbent (Hu and Xu, 2020). Physical adsorption occurs when intermolecular interactions take place (e.g., Van der Waals interactions), and therefore, it is nonselective, reversible, has fast adsorption and desorption rates, and the process hardly can change the structure of the adsorbent and adsorbate (Hu and Xu, 2020, Deng et al., 2019). On the other hand, chemical adsorption is due to the formation of chemical bonds between the adsorbate and adsorbent, such as covalent and ionic bonds (Deng et al., 2019). Chemical adsorption is selective, stable, has slower adsorption and desorption rates, and can impact the structure of the adsorbate and adsorbent (Hu and Xu, 2020).

Adsorbent regeneration is as crucial as the other desirable adsorbent characteristics in order to achieve an environmentally friendly and economic adsorption process (Kulkarni and Kaware, 2014). Several regenerative routes have been used to regenerate adsorbents, such as thermal, microbial, electrochemical, and chemical methods (Omorogie et al., 2016, Bagreev et al., 2001, Gogate and Pandit, 2004, Narbaitz and McEwen, 2012). Electrochemical oxidation is an efficient method to degrade organic matters; it is considered a safe, energy-efficient, and environmentally friendly process to regenerate adsorbents (Wang and Balasubramanian, 2009, Zhou et al., 2021). However, the efficiency of electrochemical regeneration could be reduced due to mass transfer limitations of pollutants between electrodes and the destruction of adsorbents in the process (Kang et al., 2021, Omorogie et al., 2016). Furthermore, the products resulting from the electrochemical oxidation of organics need to be identified, and cleaner energy sources of electricity should be

chosen to provide a significant environmental improvement and achieve an entire environmentally friendly treatment process.

The hybridized approach of adsorption with electrochemical oxidation of organics has gain attention due to several advantages, including safety, cost-effectiveness, operating at room temperatures and pressure, and environmentally friendly route to degrade and destroy the adsorbed organics and regenerate adsorbents (Wang and Balasubramanian, 2009, Zhou et al., 2021). The use of adsorption only cannot eliminate and destroy the pollutants present in wastewater but rather concentrate the contaminants on the adsorbent and separate them from the system (Yahya et al., 2018). This contributes towards increasing the efficiency of the electrochemical oxidation by concentrating the adsorbed organics at the anode, thus, overcoming the mass transfer limitations of pollutants between electrodes.

Several adsorbents such as activated carbon, graphene, carbon nanotubes, zeolites, and metal oxides have been used for the treatment of wastewater (Nagpal and Kakkar, 2019, Zhang et al., 2016, Sabzehmeidani et al., 2021). Activated carbon is one of the most used adsorbents due to its high surface area and high porosity (Johnson, 2014). However, the regeneration of activated carbon is typically done via thermal regeneration at high temperatures (700 – 1000 °C), which consume high energy and cause adsorbent mass loss (Sheintuch and Matatov-Meytal, 1999, McQuillan, 2021). Alternatively, lower energy consumption with higher regeneration efficiencies can be achieved for activated carbon when electrochemical regeneration is employed (Ferrández-Gómez et al., 2021). Biodegradable adsorbents such as cellulose and its derivatives are environmentally friendly with desired properties, including ease of surface functionalization and

biocompatibility (Carpenter et al., 2015). They have been proven to have excellent performance in contaminant removal owing to their oxygen-containing functional groups, including heavy metals (Sun et al., 2014), organic and inorganic pollutants (Bonenfant et al., 2010, Hokkanen et al., 2014, Zhou et al., 2013), and gas separation (Ahmad et al., 2014).

3D structured materials, such as cryogels, can increase the efficiency of the adsorption process since they have the desirable properties for the adsorption process, such as high surface area, ease of separation from treated water, ease of functionalization, and mechanical properties (Hamaker, 1937, Lipp and Körber, 1993, Corte, 1963, Baimenov et al., 2020, Qu, 2008, Anjum et al., 2019). Cryogels are macroporous polymeric materials produced from gel precursors, at subzero temperatures (Plieva et al., 2008). Cryogels allow unhindered diffusion of adsorbate in different sizes with reduced pressure drop due to their interconnected macroporous structures (Lozinsky et al., 2003).

Cellulose-based cryogels have attracted extensive attention due to their low density, interconnected pores, processability, and well-defined pore morphology that can be achieved (Buchtová et al., 2019, Liu et al., 2016). However, although cellulose-based cryogels have desirable properties for adsorption, their hydrophilicity limits their usage in applications involving water (Mendoza et al., 2018, Isogai, 2018). Therefore, cellulose modification, such as hydrophobization or crosslinking, is needed for cellulose to be used in such applications (Dilamian and Noroozi, 2021, Cervin et al., 2012, Korhonen et al., 2011).

Several carbon-based 3D structured materials have been employed for adsorption and electrochemical regeneration (Andrés García et al., 2018, Lv et al., 2009, Canencia et al., 2017). The 3D structuring of nanoparticles, such as 3D structuring of graphene, can adversely affect the unique properties of graphene, impairing its electronic, mechanical, and microstructural properties (Almazán-Almazán et al., 2009, Chandrasekaran et al., 2021, Yousefi et al., 2019). Therefore, understanding the synthesis mechanism and the effect of each parameter can lead to better optimization of 3D structured adsorbents with minimal changes in the active material's unique properties.

Despite that, 3D structured carbon-based adsorbents can effectively adsorb contaminants and be regenerated electrochemically. However, electrochemical regeneration often negatively impacts the adsorption performance of the 3D structured materials, mainly attributed to pore destruction and corrosion (Kang et al., 2021). Therefore, synthesizing an environmentally friendly 3D structured cryogel with long-term stability remains a challenge.

1.2 Thesis objective

The main objective of this thesis work was to derive sustainable and efficient hydrophobic 3D structured adsorbents through a simple and scalable route. The cryogel is composed of 2,2,6,6-tetramethyl piperidine-1-oxyl, radical (TEMPO) oxidized cellulose nanofibers (TOCN), electrochemically exfoliated graphene (EEG), and oleic acid (OA). The use of these derived cryogels to remove contaminants eliminate the need for filtration required for particle adsorbents, thus reducing the time needed for regeneration and adsorbent synthesis.

To achieve this goal, a systematic approach of linking precursor gel microstructure and rheology to the resulting cryogel's morphology and adsorption/electrochemical regeneration efficiency was taken. The main tasks required to achieve this goal were as follows:

1- Hydrophobization of TOCN (HTOCN) with OA and striking a balance between hydrophobization and microstructural properties.
2- Development of HTOCN/EEG cryogels; understand the effect of EEG loading and initial solids content on the gel network strength and their impact on the pore morphology and flexibility of the derived cryogels.
3- Test the HTOCN/EEG cryogels prepared at different EEG loadings and initial solids content for the adsorption of methylene blue organic dye. Study the effect of EEG loadings and solids content on the adsorption performance, and connect the changes that occurred from changing the parameters to the adsorption performance; Adsorption was evaluated using Langmuir adsorption isotherm and connected to the results from the previous objective.
4- Test the cryogels for the adsorption and electrochemical regeneration cycles, and evaluate the impact of electrochemical regeneration on the cryogels structure and maximum adsorption capacity.

1.3 Thesis outline

This thesis has 4 chapters, organized as follows; Chapter 1 includes an introduction, Chapter 2 includes a literature review of preparation of cryogels, applications of cryogels, factors affecting cryogels properties, cellulose nanofibers, adsorption and electrochemical oxidation for organic dyes removal. Chapter 3 presents a paper entitled "Biodegradable Cryogels for Adsorption and Electrochemical Oxidation of Dissolved Organic Dyes" to be submitted for publication. Chapter 4 gives an overview of the significant findings and conclusions, and suggestions for future work.

Chapter 2

Literature review

2.1 Preparation of cryogels

A cryogel is a 3D structured material synthesized typically through polymerization, cross-linking, and the use of gels such as biopolymers (Okay, 2014). The cross-linking route, illustrated in Figure 2-1 (Kumar et al., 2010), starts with dispersing the precursor solute in an aqueous solvent, following by freezing at a subzero temperature. During the freezing process, phase separation occurs, forming two phases: the frozen solvent phase and the unfrozen particles and solute phase (Reddy et al., 2013, Kumar et al., 2010). The solute particles start interacting to form a polymer, and once the cross-linking has completed, the cryogel is generally dried in a freeze dryer to sublimate the frozen solvent phase (Tamon et al., 2001). The polymerization route, such as free radical reaction, is used to produce polymer chains, resulting in an interconnected macroporous cryogel upon freeze-drying (Carvalho et al., 2014). Both polymerization and cross-linking routes require the addition of chemicals and the adjustment of preparation conditions, such as pH and temperature, for the reactions to occur (Kumar et al., 2010, Savina et al., 2016). The third route can be achieved by freezing followed by freeze-drying of a polymer gel (e.g., tempo oxidized cellulose nanofibers) (Pan et al., 2021). The use of freeze drying in the final stages of cryogels preparation sublimate the frozen solvent at reduced temperature and pressure, thus, preventing shrinkage and causing minimal disturbances in the pores network formed upon freezing, compared to, for example, oven drying (Guo et al., 2019, Tamon et al., 2001, Shlyakhtin and Oh, 2008). In all routes, phase separation occurs upon freezing, and the frozen solvent acts as a porogen, which unveils an interconnected, highly porous network upon drying, surrounded by walls that are created from the unfrozen polymer and particles phase (Lozinsky et al., 2003).

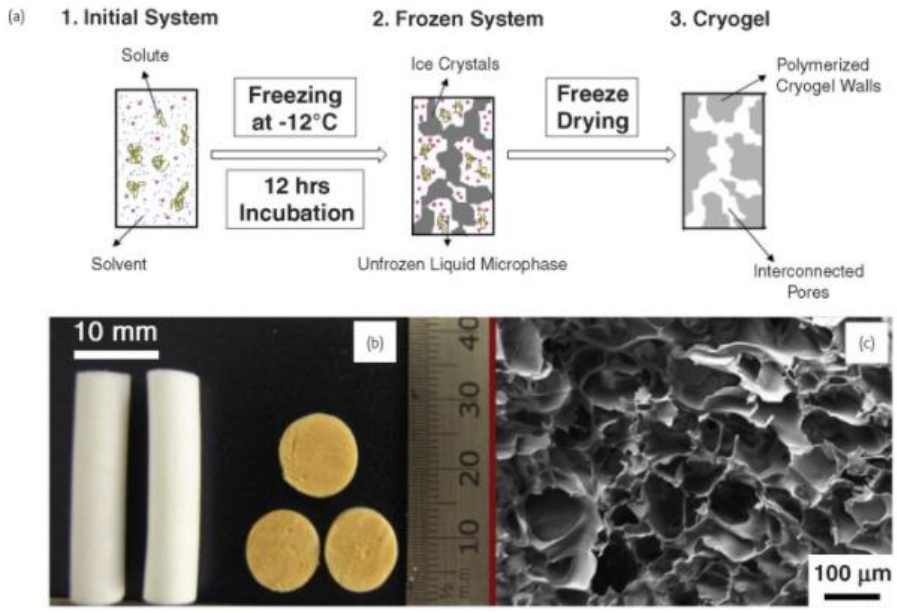

Figure 2-1 a) Cryogel preparation process, b) images of cryogels in different shapes, and c) Cryogels' scanning electron microscopy images showing its pores interconnectivity (Kumar et al., 2010).

Embedding nanoparticles in the precursor sols or gels is an efficient way to produce composite cryogels with enhanced properties (Hosseini et al., 2020). Composite cryogels possess enhanced properties that can be tuned to fit the application of interest (Memic et al., 2019). For instance, graphene oxide/cellulose composite cryogels were reported to have enhanced mechanical strength and adsorption capacity compared to cellulose cryogels due to the presence of graphene oxide adsorption sites and the increased surface area of the composite cryogel (Tang et al., 2019, Hosseini et al., 2020). The initial graphene oxide loading in the cellulose precursor sol is a crucial factor that impacts the final composite cryogels' properties such as porosity, degree of swelling, thermal properties, density, and surface area (Gan et al., 2018). Yao et al. (Yao et al., 2014) studied the effect of graphene oxide loading on the rheological properties of cellulose carbamate/graphene oxide sols. The authors concluded that graphene oxide loading influences the interaction with

cellulose and orient itself differently within the cellulose network at different loadings (Figure 2-2), altering the sols' strengths and the final cryogels' properties.

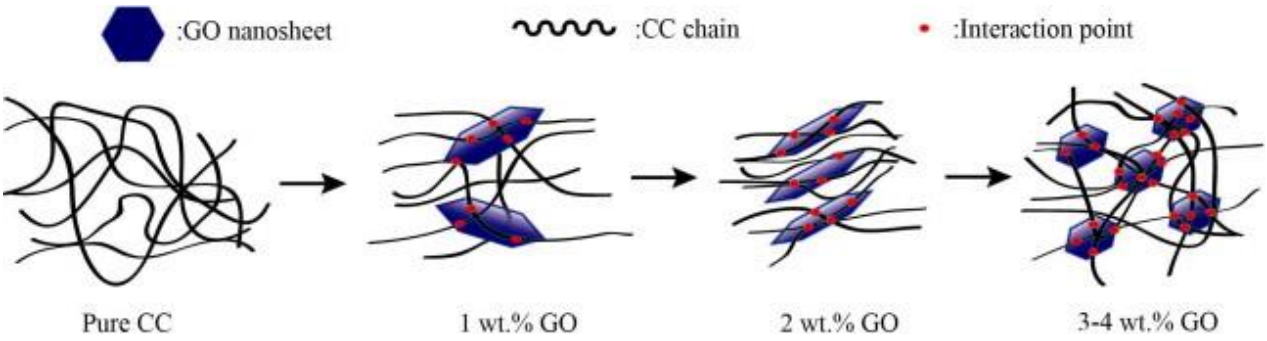

Figure 2-2 Schematic of Graphene oxide (GO) interactions with Cellulose carbamate (CC) at different GO loadings (Yao et al., 2014).

2.2 Applications of cryogels

Cryogels have gained increasing attention in different applications due to their unique characteristics that can be achieved based on the application requirements and are mostly tuned. The choice of the precursor dispersion components is usually based on the application of interest, and different components and synthesis conditions of precursor dispersion give different final properties to the cryogels (Baimenov et al., 2020).

Various materials such as polyethylene glycol (Bruns et al., 2018), poly(vinyl alcohol) (Lozinsky and Plieva, 1998), cellulose (Petrov et al., 2006), and silica (Su et al., 2012) have been employed to fabricate cryogels. Polyethylene glycol and poly(vinyl alcohol) are commonly used polymers for cryogels fabrication for biomedical applications due to their biodegradability (Memic et al., 2019). Polyethylene glycol cryogels have swelling properties, and their properties can be

controlled to fit different applications (Imaninezhad et al., 2019). The properties of poly(vinyl alcohol) cryogels can also be tuned, by changing polymer concentration, composition, and freezing conditions to obtain cryogels with different structural, physical, and chemical properties (Pazos et al., 2009).

Cryogels composed of cellulose nanofibers have been extensively studied due to their favorable properties, such as ease of functionalization, tunable porosity, mechanical stability, low bulk density, high surface area, and cellulose availability and biodegradability (Ciolacu et al., 2016, Buchtová et al., 2019, Tyshkunova et al., 2021). Due to their properties, cellulose cryogels have been employed in several applications, such as adsorption, bio-medical applications, thermal insulators, and energy storage (Ramirez et al., 2021, Ciolacu et al., 2016, Moosavi et al., 2020).

Silica cryogels are mainly produced using the sol-gel method, and they exhibit low bulk density, high surface area, high pore volume, and have excellent thermal and electric insulating properties (Gurav et al., 2010, Kistler, 1931). The resulting silica cryogels are monoliths with interconnected pores, making them suitable for various applications such as adsorption, catalysis, energy storage, and sensors in their original and modified forms (Pan et al., 2021, Su et al., 2012, Pons et al., 2012). The sol-gel method used to prepare silica cryogels might involve several steps: sol preparation, solvent exchange, aging, gelation, drying, and post-processing (Pajonk et al., 1990, Gurav et al., 2010).

Cryogels tunable properties and the various available materials used as building blocks for structuring cyogels have broadened their use in different applications. The possible applications, along with some reported building blocks materials for cryogels synthesis, are described in Table 2-1:

Table 2-1 Summary of cryogels' possible applications and their desirable properties.

Application	Examples	Desirable properties	Reference
Adsorption	poly(vinyl alcohol) Cellulose poly(N-isopropylacrylamide)	Selectivity, high porosity, low-pressure drop, high adsorption capacity/surface area, regeneration capability, and mechanical properties.	(Ivanov et al., 2012, Lazzari et al., 2019, Liu et al., 2011)
Energy storage	Carbon-based	High conductivity, high thermal stability, pore structure, high surface area, and mechanical stability.	(Li et al., 2017, Milakin et al., 2020, Kalijadis et al., 2020)
Biomedical	Gelatin polyethylene glycol	High porosity, large pores, biocompatibility, mechanical stability, and rapid swelling.	(Saylan and Denizli, 2019, Razavi et al., 2019, Liao et al., 2016, Kemençe and Bölgen, 2017)
Sensors	poly(N-isopropylacrylamide) Polyethyleneimine	High porosity, sensitivity, flexibility, shape recovery, and conductivity.	(Demirci and Sahiner, 2020, Deng et al., 2018)

2.3 Factors affecting cryogels properties

While the materials used to create cryogels have the most impact on the resultant properties, factors influencing the precursor dispersion conditions can play a significant role in determining the final properties of the cryogel. These parameters, such as concentrations/loadings, ionic strength, pH, freezing conditions, and drying method, were reported to give different cryogel properties even at slight modifications of operational conditions (Dobritoiu and Patachia, 2013, Deville et al., 2010, Porter et al., 2014, Deville et al., 2011, Mukai et al., 2008, Zhang et al., 2013, Gun'ko et al., 2013).

The effect of the solvent medium was studied by Tang et al. (Tang et al., 2016). They investigated the impact of tert-butyl alcohol content on a cryogel derived from dispersions of aluminum oxide particles in tert-butyl alcohol and water. The authors found that cryogels with different pore morphologies and mechanical properties can be obtained upon increasing the tert-butyl alcohol loading in the dispersion by 10 wt.%.

Furthermore, the precursor sol's viscosity and particle concentrations within the sol were reported to impact the ice crystal growth during the freezing stage, ultimately affecting the properties of the resultant cryogel (Wegst et al., 2010, Landi et al., 2013). Deville et al. (Deville et al., 2007) investigated the effect of ceramic content on the final morphology and found that increasing ceramic content to above 80 wt.% results in an irregular pore morphology that is not interconnected, while lower loadings produce lamellar, interconnected pores, due to particle-ice crystals interactions (Deville et al., 2006).

The solvent and particle concentration impacts the properties of the resultant cryogel by altering the interactions in the sol and the formation of the ice crystals (Deville et al., 2006, Schvezov and Weinberg, 1985). The particle-ice crystals interactions determine the porosity of the cryogels, in

which particles at higher loadings interact with ice crystals to a high extent, thus disturbing the ice crystals formation and creating a random ice growth, ultimately losing the open and interconnected pore structure of the cryrogel (Deville et al., 2006).

The pH of the frozen sol also impacts the particle-ice interactions, and therefore, can alter the pore size/shape and properties of the cryogel (Amaral-Labat et al., 2012, Hamano et al., 2014, Pan et al., 2021). Pan et al. (Pan et al., 2021) reported a systematic study investigating the effect of altering the pH of tempo oxidized cellulose nanofibers (TOCN) and graphene oxide sols on the ice crystal growth and final properties of the composite cryogel (Figure 2-3). They concluded that the pH varies the interaction of TOCN and graphene oxide with the ice crystals, which results in irregular, honeycomb, and lamella structures at pH of 4, 5.2, and 6.4-10.4, respectively. The irregular pore structure obtained at a pH of 4 was attributed to the graphene oxide aggregates at such a low pH, which disturbs the ice crystal growth. In contrast, at higher pH, the ionization of oxygen-containing groups occurs at different pH, thus altering the interaction between the components and the ice crystals. The change in pH alters the interaction in the wet gel, orienting TOCNand graphene oxide differently on the ice crystals driven by the interactions, and ultimately changing the pore morphology.

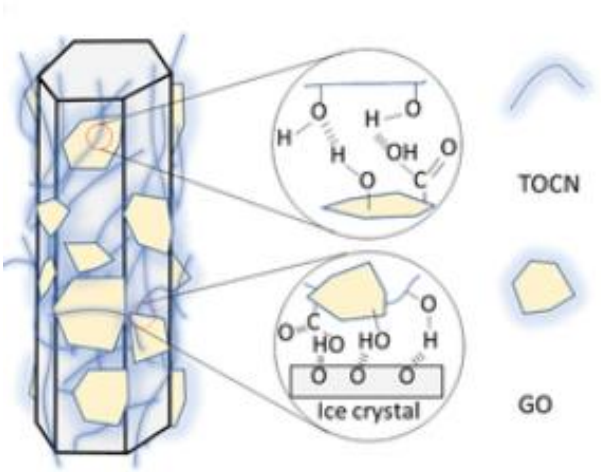

Figure 2-3 Proposed mechanism of ice crystals growth during the unidirectional freezing process of TOCNand graphene oxide sol (Pan et al., 2021).

The freezing rate was also viewed as a weighty factor, of which slower rates are most likely to create larger pores with enhanced pore interconnectivity. In comparison, faster rates result in smaller pores and lower pore interconnectivity (Kumar, 2016). The rate of freezing controls the forming ice crystal size and morphology of the resultant cryogel. Fast rates and lower freezing temperatures result in the formation of a large number of tiny ice crystals, forming small pores in the cryogel when dried. In comparison, lower freezing rates and higher temperatures lead to large ice crystals, creating large pores in the cryogel upon drying (Jiang et al., 2015). Oelschlaeger et al. (Oelschlaeger et al., 2016) studied the effect of freezing temperature on the pore morphology of hyaluronic acid/ethylene glycol diglycidyl ether cryogels at two different temperatures; −15 and −18 °C. They observed a decrease in the pore size and wall thickness (Figure 2-4) at a slightly lower temperature due to the faster formation of ice crystals, resulting in smaller ice crystals that form smaller pores upon drying. The average pore size decreased from 233 ± 50 μm to 136 ± 35

μm while the average wall thickness decreased from about 40-100 μm to about 20 μm as the cryogels are frozen at a slightly lower temperature (-18 ℃).

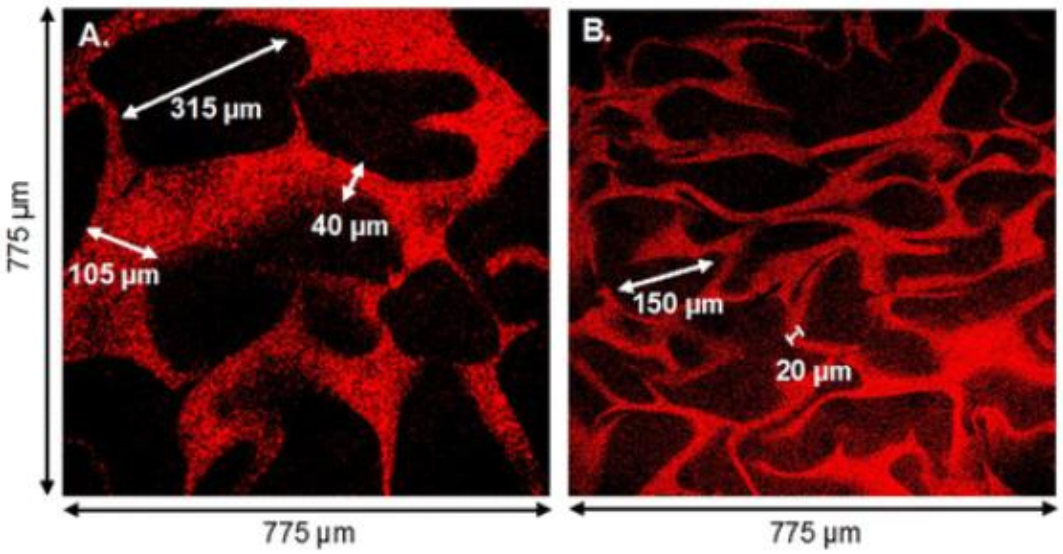

Figure 2-4 LSCM images of hyaluronic acid/ethylene glycol diglycidyl ether cryogels prepared at two different temperatures a) -15 ℃ and b) -18 ℃ (Oelschlaeger et al., 2016).

2.4 Cellulose nanofibers

Cellulose is a biopolymer, which can be derived from plants, consists of linear chains of anhydroglucose rings with the formula of $(C_6H_{10}O_5)_n$ covalently linked to each other by C-O-C and hydrogen bonds (Guan et al., 2020, Zhang et al., 2019). Cellulose is one of the most abundant and sustainable biopolymers on earth that has versatile uses in various industries like wood, paper, biomedical, food additives, membranes, etc., in its original and chemically modified forms (Liu et al., 2021a, Seddiqi et al., 2021, Zhang et al., 2019).

Tempo oxidized cellulose nanofibers

2,2,6,6-tetramethyl piperidine-1-oxyl, radical (TEMPO)-oxidized cellulose nanofibers (TOCN) is a modified type of cellulose nanofibers obtained via the oxidation of cellulose with TEMPO, sodium hypochlorite, and sodium bromide to mainly convert the C6 hydroxyl group to carboxylate group (Saito et al., 2006, Saito and Isogai, 2004), as shown in Figure 2-5. The oxidation of cellulose to TOCN has open doors for more applications of cellulose due to the properties of TOCN (Rahmatika et al., 2019, Saito et al., 2007), including:

1) Homogenous fibers width of about 3 nm and a high aspect ratio, higher than 150.
2) High carboxyl content leads to a good dispersion in water due to the highly negative charge caused by the electrostatic repulsion between TOCN.
3) TOCN has a high affinity towards positively charged compounds owing to its carboxyl groups, making it suitable for adsorption applications.

Figure 2-5 Cellulose oxidation to 2,2,6,6-tetramethyl piperidine-1-oxyl, radical (TEMPO)-oxidized cellulose nanofibers (TOCN) (Kotatha and Rungrodnimitchai, 2018).

TOCN nanofibers are water-dispersible, have hydroxyl and carboxylic groups, and form a hydrophilic cryogel when freeze-dried at a concentration higher than 0.1 wt.% (Mendoza et al., 2018, Isogai, 2018). The 0.1 wt.% dispersion corresponds to the onset of gelation, thus, creating a network upon freezing. This low concentration allows the minimization of TOCN loadings in the cryogel, if needed. Nonetheless, TOCN in its original hydrophilic form, in general, requires no further processing to produce cryogels, such as aging or gelation steps, ultimately requiring less processing time as opposed to, for example, the sol-gel method that is needed for silica cryogels/aerogels.

Hydrophobization of TOCN

Due to TOCN hydrophilicity, several methods have been reported in the literature for the hydrophobization of cellulose nanofibers and its derivatives to broaden its usability, including esterification, silanization, and the use of fatty acids such as oleic acid (Chen et al., 2015, Abdul Khalil et al., 2014, Lazzari et al., 2017).

The use of oleic acid to hydrophobize cellulose and particles is a simple method that does not require long processing times or high temperatures (Rai, 2020, Chen et al., 2015). Chen et al. (Chen et al., 2015) studied the effect of oleic acid loading on the hydrophobization of cellulose films functionalized with sulfate groups. They observed an increase in contact angle with increasing oleic acid loadings, suggesting the dependency of the hydrophobicity on oleic acid loading. Furthermore, they reported an increase in the viscosity of the gel due to the interaction between the oxygen-containing groups on oleic acid and cellulose. The viscosity was found to increase with

increasing oleic acid loadings until an excess amount of oleic acid is added that is not interacting but causing phase separation, resulting in viscosity drop.

2.5 Adsorption and electrochemical oxidation for organic dyes removal

Adsorption

Adsorption is one of the most used methods for wastewater treatment applications due to its simplicity, low cost, and high efficiency (Sabzehmeidani et al., 2021). Adsorption is the adhesion of atoms and molecules from the fluid phase onto the surface of the adsorbent. The adsorption consists of three mechanisms that occur in consecutive steps, described in Table 2-2 (Zhu et al., 2020, Karimi et al., 2019) and illustrated in Figure 2-6.

Table 2-2 Adsorption mechanism and the determining parameters.

Type	Mechanism	Notes
External diffusion	Transfer of substances from the bulk liquid phase to the adsorbents' exterior surface.	Exterior surface area determines the rate.
Internal pore diffusion	Transfer of substances from exterior to interior surface (pores and pore walls).	Pore structure and pore volume are dominant factors.
Adsorption	Takes place on the active sites within the adsorbent.	External and internal diffusions determine the adsorption rate.

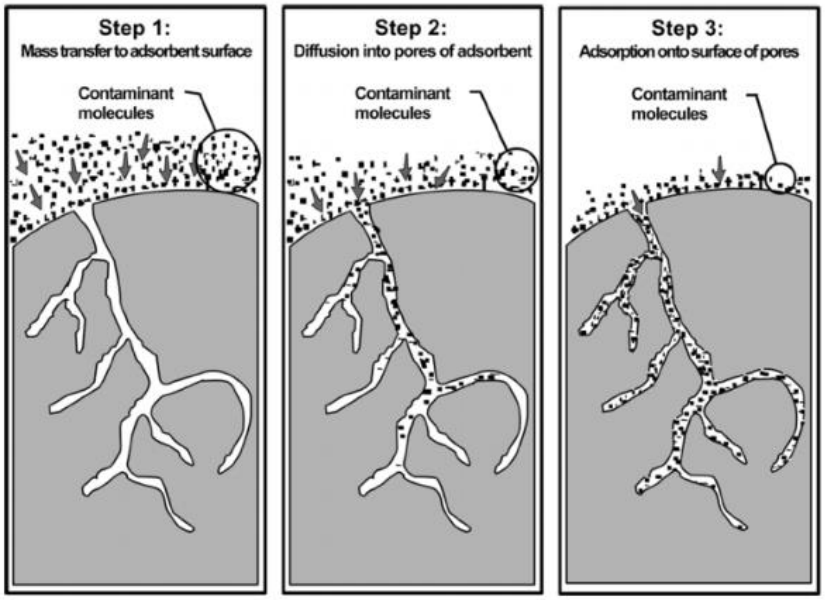

Figure 2-6 Illustration of adsorption on porous adsorbent (Connors et al., 2013)

Adsorption is often characterized by adsorption isotherms, which show the relationship at equilibrium between the adsorbed amount on the surface of adsorbent and the residual adsorbate amount in the liquid phase at constant temperature (Mourabet et al., 2011). The equilibrium adsorption isotherm is essential and provides information about adsorption (e.g., adsorption capacity and affinity). Several models, such as Langmuir and Freundlich adsorption isotherms, were established to understand different adsorption systems under different assumptions and theories (Freundlich, 1906, Langmuir, 1918, Worch, 2012).

The experimental adsorption uptake (Q_e, mg/g) in batch adsorption experiments can be determined by the mass balance equation shown below (Ramaswamy et al., 2013):

$$Q_e = \frac{V(C_o - C_e)}{m} \qquad \text{Equation 1}$$

where V is the volume of solution (L), C_o is the initial concentration of adsorbate in the solution (mg/L), C_e is the final concentration of adsorbate at equilibrium (mg/L), and m is the mass of adsorbent (g).

The Langmuir adsorption isotherm (Equation 2) is a theoretical model that relies on the assumption that the adsorption is monolayer on the adsorbent with adsorption sites having homogenous adsorption energy (Worch, 2012).

$$Q_e = \frac{Q_m K_L C_e}{1 + K_L C_e} \qquad \text{Equation 2}$$

where Q_m and K_L are the adsorption model parameters, maximum adsorption capacity (mg/g) and the Langmuir constant (L/mg), respectively, C_e is the equilibrium concentration of MB (mg/L).

The Langmuir model is not applicable in cases where the previously mentioned assumptions are not fulfilled (Worch, 2012, Langmuir, 1918). The Freundlich model was proposed in 1906, and it assumes a heterogeneous adsorbent surface with different actives sites' energy and multiple adsorption coverage (Ayawei et al., 2017, Worch, 2012). The Freundlich model does not estimate the maximum adsorption capacity, but it gives information about the adsorption mechanism instead (Sparks, 2003).

$$Q_e = K C_e^n \qquad \text{Equation 3}$$

where K and n are the adsorption model parameters. K is the adsorption coefficient (L/mg), and n is the correction factor related to the energetic heterogeneity of the adsorption sites (dimensionless). Although the Freundlich model cannot predict the maximum adsorption capacity, but the higher is the K value, the higher is adsorbent capacity (Worch, 2012). The n value gives information about the favorability of the adsorption; values higher than one are characterized as

unfavorable adsorption while lower than one is favorable and suggests high adsorption uptakes at low concentrations of the adsorbate (Worch, 2012).

Electrochemical oxidation/regeneration

The regeneration of adsorbents is crucial to ensure sustainability and eco-friendly treatment methods. Several regenerative routes have been reported to regenerate adsorbents, such as electrochemical regeneration, thermal regeneration, bio-regeneration, and chemical methods (Pan et al., 2018a, Labiadh and Kamali, 2020, El Gamal et al., 2018, Labiadh and Kamali, 2019). Thermal regeneration is one of the most used regeneration techniques in industrial applications, and it requires high energy consumption and often causes adsorbent mass loss (McQuillan, 2021, Sheintuch and Matatov-Meytal, 1999, Sharif et al., 2017). Bio-regeneration involves the use of microbes to break down the organic contaminants into simpler molecules like CO_2 and methane (El Gamal et al., 2018).

The electrochemical regeneration process is related to the changes induced by the electric current . It is considered an environmentally friendly, safe, and energy-efficient approach to degrade organic pollutants and regenerate adsorbents (Wang and Balasubramanian, 2009, Zhou et al., 2021). This method has been used for the removal and degradation of different organic contaminants from contaminated water, such as organic dyes (Panizza et al., 2007, Yi et al., 2008), methanol (Yao et al., 2021), phenol (Abou-Taleb et al., 2021), and many other pollutants (Pierpaoli et al., 2021, Zhu et al., 2021, Wu et al., 2021, Yu et al., 2021). Electrochemical regeneration involves two possible oxidations routes, direct and indirect oxidation, illustrated in Figure 2-7 (Martínez-Huitle and Ferro, 2006).

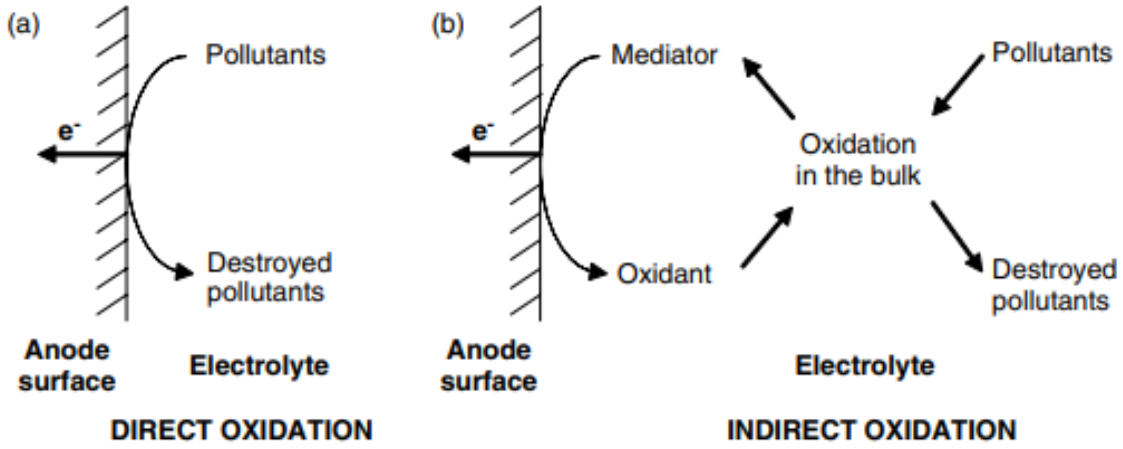

Figure 2-7 Scheme of direct (a) and indirect (b) oxidations of pollutants (Anglada et al., 2009).

Direct oxidation occurs by the in-situ produced hydroxyl radicals and direct electron transfer, with an efficiency dependent on the electrode material (Iniesta et al., 2001). The produced radicals during the direct oxidation oxidize the organic pollutants, according to the following electrochemical reactions (M is the anode material while R is the fraction of an organic compound) (Martínez-Huitle and Ferro, 2006):

$$M + H_2O \rightarrow M(^{\bullet}OH) + H^+ + e^-$$

$$R + M(^{\bullet}OH) \rightarrow M + CO_2 + H_2O$$

The electrode material impacts the overall efficiency of the oxidation process; therefore, it must be chosen carefully; preferably include the following properties (Anglada et al., 2009):

1) Chemically and physically stable with low cost, showing high resistance to corrosion and erosion.
2) Sufficient electric conductivity.

3) Selectivity towards the oxidation of organics at the anode surface rather than the oxygen evolution side reaction, shown below:

$$2H_2O \rightarrow O_2 + 4H^+ + 4e^-$$

The high competition between organic oxidation and oxygen evolution reaction results in the need for longer treatment times due to the reduction in current efficiency. The increasing competition could be attributed to the low concentration of the pollutant and the nature of anode material and pollutants (Vargas et al., 2016, Martínez-Huitle and Ferro, 2006).

Indirect electrochemical oxidation generates a strong oxidizing agent at the anode surface that destroys pollutants presented in the bulk solution. However, such an approach might produce more toxic compounds than the starting compounds. For instance, sodium chloride is one of the most powerful electrolytes used for oxidizing pollutants; however, it produces chlorine and hypochlorous acid or hypochlorite, depending on the pH; these byproducts are toxic and might be seriously harmful, as per the following reactions (Scialdone et al., 2009):

$$2Cl^- \rightarrow Cl_2 + 2e^-$$

$$Cl_2 + H_2O \rightarrow HOCl + H^+ + Cl^-$$

$$HOCl \leftrightarrow H^+ + OCl^-$$

Chapter 3

Biodegradable Cryogels for Adsorption and Electrochemical Oxidation of Dissolved Organic Dyes

Statement of contribution: Saqr Abuhatab: performed all the experiments related to cryogel fabrication and consequent characterization, adsorption and regeneration experiments, performed analysis, wrote the original draft, and performed revisions/edits. Milana Trifkovic: Intellectual input, conceptualization of the work, paper/thesis review and edits, along with supervision. Edward Roberts was involved in discussions, intellectual input, and paper revisions. Fernanda Lopez synthesized graphene for this work. Aleksandra Govedarica helped with the confocal imaging protocol. Ashutosh Singh helped with the regeneration setup.

Abstract

The present work demonstrates an innovative strategy to fabricate a robust biodegradable cryogel for the removal of dissolved organic contaminants, followed by its successful regeneration by electrochemical oxidation. The cryogels were fabricated by mixing aqueous dispersions of 2,2,6,6-tetramethyl piperidine-1-oxyl, radical (TEMPO) oxidized cellulose nanofibers (TOCN), oleic acid (OA), and electrochemically exfoliated graphene (EEG) nanoplatelets at 50 °C, followed by their freeze-drying. Hydrophobization of TOCN with OA (HTOCN) allowed utilization of the derived cryogels in aqueous environments. A combination of confocal microscopy and rheology was utilized to investigate the effect of precursor gel composition in terms of HTOCN to EEG weight ratio (1:1 and 1:2) and total solids content (varying from 1 wt.% to 6 wt.%), by analyzing the microscopic details of HTOCN distribution and connecting it to the gel's macroscopic flow

behavior. The spatial distribution of HTOCN domains shows a clear dependence on the HTOCN/EEG ratio. Interestingly, we found that HTOCN/EEG 1:2 gel with 6 wt.% solids content has the largest HTOCN domains and exhibits at least an order of magnitude higher storage/loss modulus than any other investigated gel, indicating that the enhancement in the rheological signature could arise from the more pronounced $\pi-\pi$ stacking of EEG nanoplatelets at higher EEG loadings. SEM images of the derived cryogels confirmed the presence of EEG aggregates whenever the EEG loading in the precursor gel is higher than 2 wt.%. The adsorption capacity of the derived cryogels is largely affected by their microscopic arrangements. As expected, increasing EEG content in the precursor gel leads to higher adsorption capacity, but the upturn in adsorption capacity is highly dependent on the level of EEG aggregation, corresponding to the accessible surface area for adsorption of methylene blue dye. All cryogels showed excellent stability during multiple adsorption/electrochemical regeneration cycles, with less than a 20% increase in the adsorption capacity after 18 consecutive cycles. Our results provide new insights into the link between the precursor gel's properties and the performance of the derived cryogels needed to design effective adsorbents for practical applications.

3.1 Introduction

Hierarchically structured 3D materials have attracted attention due to their wide scope of applications in adsorption, energy storage/conversion, tissue engineering, catalysis, insulation, and sensing; they provide large surface area and high pore volume with pore size ranging from several nanometers to hundreds of micrometers (Wu et al., 2020, Yoon et al., 2017, Estevez et al., 2018, Feng et al., 2021, Mohamed et al., 2021, Baimenov et al., 2020, Zhang et al., 2017, Farías et al., 2020). Among different approaches for fabricating porous materials, soft material templating methods have been recognized as advantageous due to their versatility, controllability, low cost, and uncomplicated synthesis procedure (Zhang and Hoshino, 2019, Davis, 2002, Li et al., 2012, Wales et al., 2015). In this regard, recent years have witnessed significant interest in the freeze-drying method towards various porous materials with tailored porosity and microscopic morphology (Groult et al., 2021, Pan et al., 2021, Liu et al., 2021b, Davis, 2002, Li et al., 2012, Wales et al., 2015). Properties of the precursor dispersion used for the freeze-drying process govern the phase separation mechanisms, resulting in porous 3D structured materials (cryogels) with different pore morphologies (e.g. regular and irregular pore shapes) and mechanical properties (Zou and Budtova, 2021, Pan et al., 2018b, Pan et al., 2016). Various factors have been reported to affect the precursor dispersion, ultimately changing the characteristics of the cryogels, including polymer and particle loading, particle size distribution, their dispersibility in solvent mediums, ionic strength, pH, mixing and aging duration, and freezing conditions (Dobritoiu and Patachia, 2013, Deville et al., 2010, Porter et al., 2014, Deville et al., 2011, Mukai et al., 2008, Zhang et al., 2013, Gun'ko et al., 2013). The combination of tunable porosity and mechanical properties, along with the simple and easily reproducible synthesis approach, make cryogels suitable for adsorption applications (Henderson et al., 2013, Lozinsky et al., 2003). Their three-

dimensional structure with the open interconnected pore morphology offers accessible pores with reduced pressure drop compared to traditional columns (e.g., packing particle adsorbent in columns) (Hajizadeh, 2012, Gun'ko et al., 2013). Several cryogels have been extensively investigated for adsorption applications, including chitosan-based (Rattanakunsong and Bunkoed, 2020, García-González et al., 2021, Yin et al., 2021), cellulose-based (Toledo et al., 2019, Lazzari et al., 2019, Kunz Lazzari et al., 2021), polyacrylamide-based (Cristina Oliveira Neves et al., 2020, Marcuz et al., 2021), graphene oxide/poly (*N*-isopropyl acrylamide-maleic acid) (Yang et al., 2020), poly(vinyl imidazole) (Zhong et al., 2020), and carboxymethyl cellulose-based cryogels (Li et al., 2020).

While cryogels hold great promise as adsorbents, their efficiency is highly dependent on the structural integrity and long-term stability in harsh environments that are often encountered during the regeneration process (Jayanthi et al., 2016, Zhang et al., 2017, Wang et al., 2017). Several regenerative routes have been used to regenerate adsorbents, including electrochemical (Pan et al., 2018a), thermal (Labiadh and Kamali, 2020), bio-regeneration (El Gamal et al., 2018), and chemical regeneration (Labiadh and Kamali, 2019). Thermal regeneration at temperatures between 700 – 1000 °C, is one of the most widely used regeneration techniques in industrial applications. However, this technique requires high energy consumption, and it often causes adsorbent mass loss (McQuillan, 2021, Sheintuch and Matatov-Meytal, 1999, Sharif et al., 2017). Combining adsorption with electrochemical oxidation has been found to be an environmentally friendly, safe, and energy-efficient approach to degrade organic pollutants and regenerate electrically conductive adsorbents (Wang and Balasubramanian, 2009, Zhou et al., 2021).

Adsorption-electrochemical regeneration for 3D structured materials such as: carbon/silica aerogel (Canencia et al., 2017), carbon nanosphere/graphene composite (Kang et al., 2021), carbon

aerogels (Lv et al., 2009) has been reported in the literature. The carbon/silica adsorption capacity was found to increase over the consequent cycles due to the increased surface area caused by electrochemical regeneration. On the other hand, the two other carbon-based aerogels' capacities were reported to decrease due to the destruction of pores during electrochemical regeneration (Lv et al., 2009, Kang et al., 2021). The challenges associated with electrochemical regeneration of structured adsorbents, which largely limit their application in practice, are due to the lack of their structural integrity, high contact resistance induced by the poor adhesion between an adsorbent and an electrode, and adsorbent corrosion.

Herein, we report fabrication of a novel composite cryogel for the removal of dissolved contaminants from water, with enhanced long-term stability during electrochemical regeneration. We utilize environmentally friendly precursors, namely hydrophobized 2,2,6,6-tetramethyl piperidine-1-oxyl, radical (TEMPO)-oxidized cellulose nanofibers (HTOCN) and electrochemically exfoliated graphene (EEG). The derived HTOCN/EEG cryogels have structural integrity in aqueous solutions without the need for further reduction of carboxyl groups, and offer unprecedented long-term stability withstanding 18 regeneration cycles with minimal change in adsorption capacity. We systematically investigate the weight ratio of EEG and HTOCN as well as cryogel density/solids content to achieve a balance between the adsorption capacity and structural integrity, leading to long-term stability during the electrochemical regeneration process.

3.2 Experimental Section

3.2.1 Preparation and characterization of hydrophobic TOCN

A 1 wt.% TOCN suspension with 1.5 mmol/g carboxylic content was purchased from the University of Maine, US. Oleic acid (OA, purity >99%), used for the hydrophobization of TOCN,

was purchased from Science Ward. Hydorphobized TOCN, referred to from now on as HTOCN, was prepared by simply mixing TOCN with OA with a magnetic stirrer at 50 °C and 300 rpm. TOCN/OA gels were prepared at different TOCN to OA weight ratios; 1:0.02, 1:0.05, 1:0.08, 1:0.1, and 1:0.25 (2, 5, 8, 10, and 25 wt.% of OA, respectively) to study the effect of OA loading on the strength and dispersibility of the TOCN gels. Fourier transform infrared (FTIR) spectroscopy was used to confirm hydrophobization of TOCN. Experiments were conducted using Agilent Technologies FTIR (model Cary 630) with 100 sample scans and 4 cm^{-1} resolution in the range of 400-4000 cm^{-1}.

3.2.2 Preparation of HTOCN/EEG cryogels

Electrochemically exfoliated graphene (EEG) nanoplatelets, synthesized in the presence of ammonium sulfate, were obtained using a previously reported procedure (Lopez Pablos, 2021). 40 mL of 1 wt.% and 2 wt.% EEG dispersions were prepared in deionized water (>18 MΩ cm, Milli-Q), and probe sonicated (Fisherbrand model 705 sonic dismembrator) at an amplitude of 50 Hz, using a 5 seconds pulse for a total of 4 hours, with a total energy input of ~133 kJ.

The HTOCN/EEG gels were prepared in either 1:1 weight ratio (by mixing 1 wt.% HTOCN and 1 wt.% EEG dispersions) or 1:2 ratio (by mixing 1 wt.% HTOCN and 2 wt.% EEG dispersions). The precursor gels were prepared by mixing dispersions for 1 hour on a magnetic stirrer hot plate at 300 rpm speed and a controlled temperature of 50 °C. The pH of the resultant gel was found to be near neutral ~ 6.85, with no adjustment. The final solids content of each HTOCN/EEG gel (the combined weight percent of HTOCN and EEG in the gel) was manipulated by evaporating 50 or 75 wt.% of the water content using a hot plate at 80 °C and 300 rpm prior to the freeze-drying step. The targeted water evaporation was achieved by monitoring the total mass of the sample. The final total solids content of the 1:1 HTOCN/EEG were 1%, 2%, and 4 wt.%, and 1.5%, 3%, and 6 wt.%

for the 1:2 HTOCN/EEG, after 0%, 50%, and 75 wt.% of the water content in the gels was evaporated, respectively.

For the cryogel preparation, the precursor gels were frozen in 23 mm × 23 mm × 2 mm square molds before drying for 48±1 hours in a freeze dryer (LABCONCO Benchtop Freeze Dryer, operating conditions: 0.003 mbar and –105 °C).

3.2.3 Rheological measurements

TOCN/OA and HTOCN/EEG gels' viscoelastic properties were determined using an Anton Paar Modular Compact Rheometer (MCR 302 WESP model) through oscillatory shear stress sweep measurements. The geometry used to carry out all rheological measurements was a 25 mm parallel plate with a 1 mm gap. The temperature-controlled rheological measurements were performed in a convection oven (Anton Paar CTD 450 model) in air at ambient pressure. The gels were loaded at room temperature before ramping up the temperature to 50 °C. The controlled temperature measurements were defined to begin after the temperature in the oven remains at 50 °C for 90 seconds to avoid temperature fluctuation. The oscillatory shear stress measurements were performed by ramping the stress from 0.1 to 1000 Pa, and performed at least twice to ensure the reproducibility of the results.

3.2.4 Laser scanning confocal microscopy (LSCM)

Leica SP8 TSC inverted microscope with a white laser excitation source and 8 kHz resonant scanner was used to investigate the mixed gels. Oleic acid is inherently fluorescent in the region of 420-700 nm upon exciting with different lasers; a 480 nm laser gives an emission spectrum from 500-700 nm (see Figure S1 in SI), while the emission spectrum can be extended to 420-700 nm upon exciting with a 405 nm laser (Figure S2 in SI). On the other hand, TOCN is not fluorescent, and therefore, it was tagged with Rhodamine B Isothiocyanate (RITC, 99.9%, Sigma

Aldrich) for LSCM imaging (see SI for the tagging procedure). The tagged TOCN was excited using a 550 nm laser, and the fluorescence emission was observed in the region of 565-620 nm (see Figure S1 in SI for emission spectrum).

Since OA's emission overlaps with that of tagged TOCN with RITC dye (Figure S2, SI), gating and sequential imaging in two modes was used to minimize the overlapping and noise, as follows: oleic acid was first detected using 405 nm laser with a recorded emission spectrum from 420 to 520 nm, in the second mode at 550 nm laser and 565-620 nm emission window was recorded for the tagged TOCN. 2D images of the TOCN/OA and HTOCN/EEG were obtained using a 10x magnification objective with 1024×1024 image format, 1.03 μm pixel size, 0.8 AU pinhole, 1.03 mm × 1.03 mm image size, and 400 Hz scanning speed.

3.2.5 Scanning Electron Microscopy (SEM)

HTOCN/EEG cryogels pore morphology was observed using scanning electron microscopy (SEM, Phemom^{TM}, Pro X/ Pro/ Pure model). The frozen gels were cut in halves before freeze-drying, and the dry cross-sections were examined for the pore morphology of cryogels. Samples were attached to conductive carbon adhesive tabs on an aluminum mount and imaged using 15 kV acceleration voltage and 1024 × 1024 pixel resolution.

3.2.6 Adsorption isotherms

The adsorption of methylene blue (MB) onto HTOCN/EEG cryogels and the subsequent electrochemical regeneration were performed in batch mode at room temperature. The excess MB after adsorption was analyzed using UV-Vis spectrophotometry at 664 nm wavelength (calibration curve in SI, Figure S3). The adsorption isotherm experiments were carried out by immersing a known amount of the derived cryogels in 25 mL solutions of 50-100 mg/L MB at 100 rpm for 24 hours. All adsorption experiments were performed at pH of 7 and room temperature (21 °C). The

Langmuir adsorption model was used to fit the experimental data and obtain the model parameters (maximum adsorption capacity and the Langmuir constant). The Langmuir adsorption model, mass balance equation, and error analysis are described in detail in the supporting information.

3.2.7 Electrochemical regeneration

The derived cryogels were attached to graphite electrodes using a conductive epoxy resin, obtained by mixing the epoxy with graphene nanoplatelets, as shown in Figure S4 in SI. The adsorption followed by electrochemical regeneration was performed in two consecutive steps:

1- Adsorption was carried out by immersing the derived cryogels in 50 mL solutions containing 75 mg/L MB for 24 hours at room temperature, pH 7, and 100 rpm.

2- Electrochemical regeneration was conducted in a 200 mL of 1 wt.% Na_2SO_4 solution. A constant current density of 10 mA/cm^2 applied for one hour, in galvanostatic mode, was maintained using a Metrohm Autolab potentiostat to degrade the adsorbed methylene blue dye and regenerate the cryogel (Samarghandi et al., 2020).

Steps 1 and 2 represent one adsorption-electrochemical regeneration cycle, and were repeated at the same experimental conditions throughout all cycles. The regeneration efficiencies were normalized to 100% and calculated as follows (Asghar et al., 2012):

$$R = \frac{Q_r}{Q_i} \times 100\% \qquad \text{Equation 1}$$

where Q_r and Q_i are the regenerated and initial adsorbent adsorption uptake, respectively. The change in the mass of cryogels was measured by weighing the freshly derived cryogels and performing the same after five adsorption-electrochemical regeneration cycles. The impact of electrochemical regeneration cycles on the pore morphology of the cryogels was observed using SEM. Prior to SEM imaging and measuring their weight after the adsorption-electrochemical regeneration cycles, the cryogels were first washed with DI water and freeze-dried.

3.3 Results and discussion

3.3.1 Hydrophobization and characterization of TOCN

Since OA was used for the hydrophobization of TOCN, the optimization of OA loading was the first step in the preparation of the cryogels. Figure 3-1 shows the storage (G') and loss (G") moduli of the TOCN and HTOCN at room temperature (Figure 3-1 a) and at 50 °C (Figure 3-1 b). TOCN/OA gels were prepared at the same TOCN content and mixing conditions; thus, the viscoelastic properties variation of gels is mainly attributed to OA content and temperature. Irrespective of OA loading or temperature, HTOCN gels have different linear viscoelastic envelopes (The region in which applied stress is insufficient to cause a structural breakdown of the structure) in comparison to TOCN gels. As seen from Figure 3-1, increasing OA loading results in an increase in G' and G'', as well as their crossover point (indicating critical shear stress) up to 5 wt.% of OA, while further increase in its loading results in a decrease of the same properties (see Figure S5 in SI for higher than 10 wt.% OA loadings).

Our results are consistent with the trends previously reported by Chen et al. (Chen et al., 2015); the authors concluded that the interactions (hydrogen bonding) and contact probability between OA droplets and cellulose sulfate interfacial area increase the gels' viscosity. However, increasing OA loading above a certain concentration decrease the homogeneity and viscosity of the gel due to the coalescence and formation of large droplets of OA. This aligns with our findings except that the decrease in rheological properties occurred at much lower OA loading (5 wt.%), due to the TOCN carboxyl groups content and operating near neutral pH. The interaction between OA and TOCN can occur through hydrogen bonding between carboxyl groups on both components, or between the hydroxyl groups on TOCN and the carboxyl group on OA. However, once the saturation point in terms of hydrogen bonding between TOCN and OA is reached, further increase

in OA loading is expected to lead to the formation of large OA droplets, which can disrupt the TOCN network, and therefore, reduce the G' and G'' of the gels.

The viscoelastic properties obtained from shear stress ramps of the HTOCN gels at 50 °C are depicted in Figure 3-1 b. They follow the same trend as the gels prepared at room temperature, with absolute values of G' and G'' and crossover points being slightly lower, mainly driven by the reduction in the TOCN network viscosity at elevated temperatures.

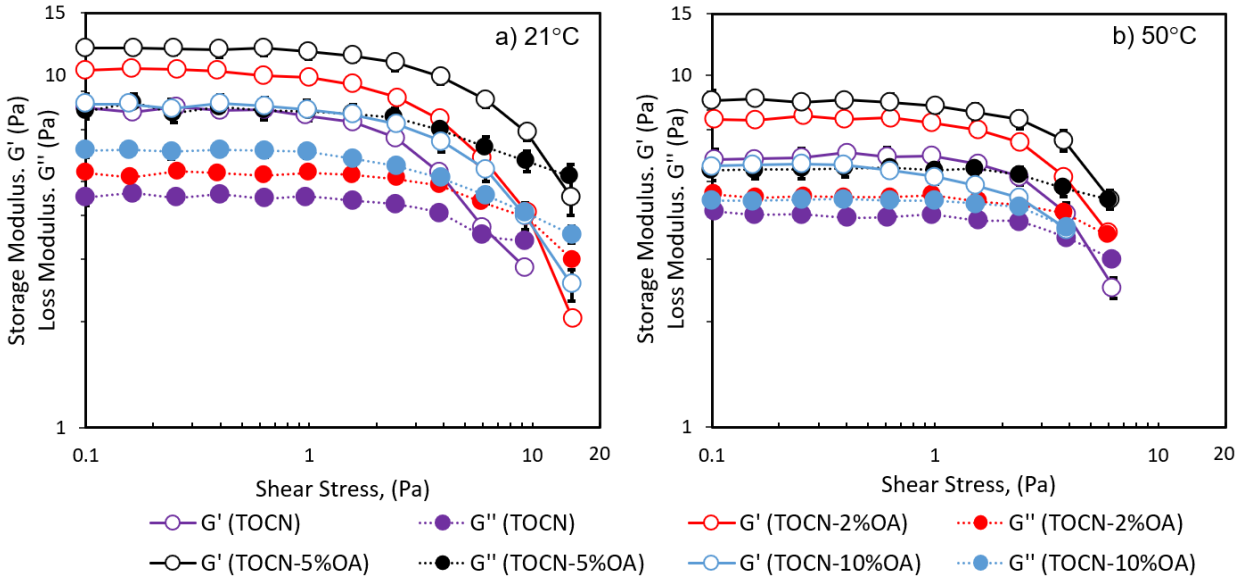

Figure 3-1 Rheological characterization of HTOCN mixed gels at different OA loadings; percentage shows the amount of OA by weight. a) Shear stress sweep at 21 ± 1 °C and b) shear stress sweep at 50 °C.

LSCM images shown in Figure 3-2, depict that gels with OA content from 2-5 wt.% had small OA droplets (< 20 μm), while increasing the OA loading to 10 wt.% resulted in the coalescence of the droplets, characterized by the presence of large (> 50 μm) OA droplets. This is consistent with the rheological signature of HTOCN gels, for which increasing the concentration above 5 wt.% reduced the strength of the gel due to the presence of large OA droplets, which cause HTOCN

network disruption. However, by increasing the temperature to 50 °C, the interfacial tension of OA/water is reduced, resulting in a decrease of the OA droplet size and enhanced probability of interaction between OA and TOCN.

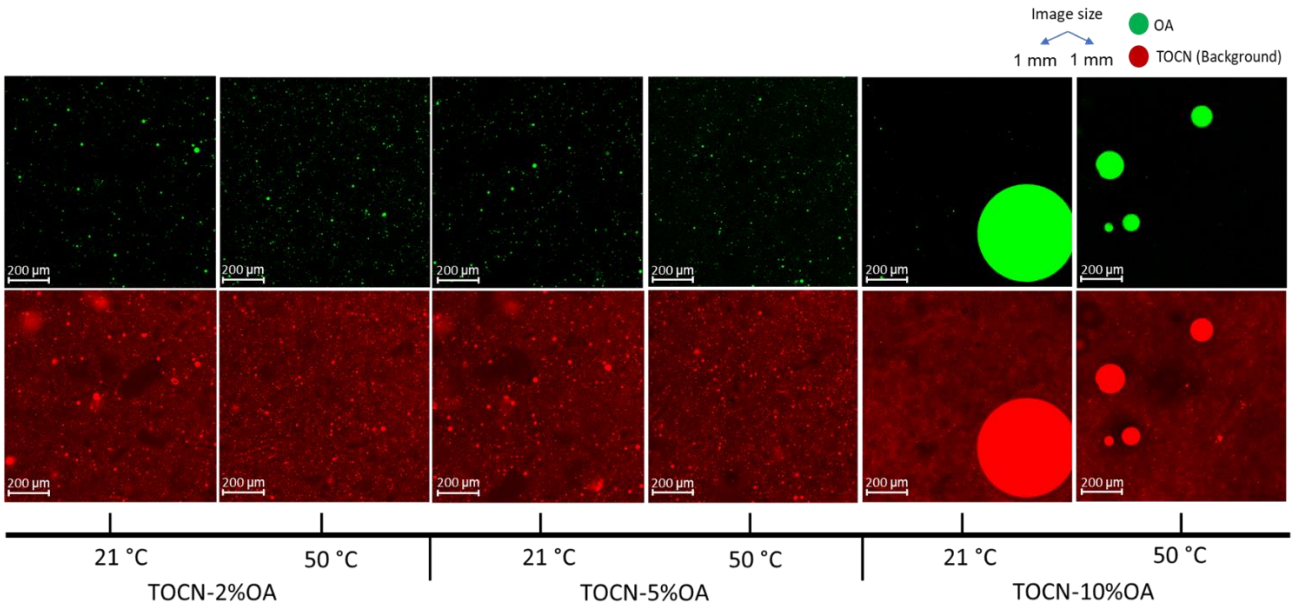

Figure 3-2 LSCM images of TOCN/OA gels at different OA loadings.

The successful hydrophobization of TOCN with OA was further confirmed by recording the FTIR spectra of the TOCN and HTOCN cryogels, shown in Figure 3-3. The characteristics of TOCN bands at 3270-3340 cm^{-1} corresponds to –OH stretching vibration, 2860-2940 cm^{-1} to $–CH_2$ groups, 1610 cm^{-1} to carboxylate group, 1430 cm^{-1} to C–H symmetrical deformation, 1113 cm^{-1} and 1048 cm^{-1} to C–O–C stretching vibration, and 891-896 cm^{-1} to cellulosic β-glycosidic linkages (Benkaddour et al., 2014, Al-Ahmed et al., 2020, Soni et al., 2015). HTOCN has the same TOCN characteristics but with additional bands at 2852 cm^{-1} and 2922 cm^{-1}, attributed to the symmetric and asymmetric CH_2 stretching in oleic acid. The band at 1710 cm^{-1} is due to C=O stretching vibration, while the band at and 1409 cm^{-1} correspond to CH_3 stretching from OA modifications (Yang et al., 2010).

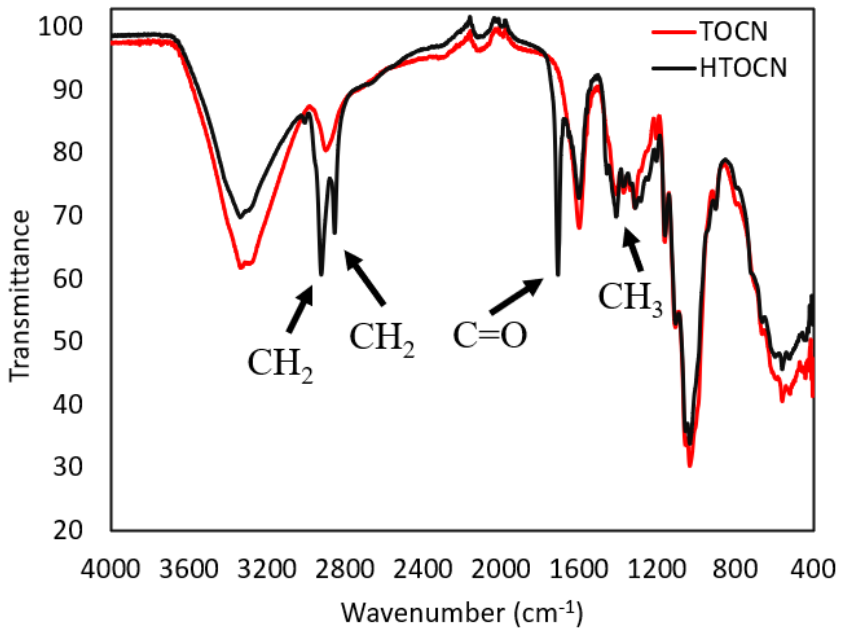

Figure 3-3 FTIR spectra for TOCN and HTOCN before and after the hydrophobization using 5 wt.% OA. The main characteristics bands of OA are shown in the figure.

3.3.2 Characterization of HTOCN/EEG gels and cryogels

The viscoelastic properties of the HTOCN/EEG precursor gel impact the mechanical properties, pore size distribution, surface area, and adsorption efficiency of the resulting cryogels obtained after freeze-drying. Figure 3-4 shows the viscoelastic properties of HTOCN/EEG mixed gels obtained as a function of HTOCN/EEG ratio and solids content. Interestingly, G' and G'' increased slightly when the EEG loading was doubled, in the absence of any water evaporation. However, the G' and G'' of the 1:2 HTOCN/EEG gels obtained after 50% and 75 wt.% water evaporation were almost two orders of magnitude higher in comparison to the 1:1 HTOCN/EEG gels. While the solids content in 1:2 HTOCN/EEG gels was 50% higher for all gels at each water evaporation percentage, the drastic increase in the network strength induced by evaporation of 1:2 gels indicates the enhanced interaction between HTOCN and EEG enabled by longer exposure to mixing at elevated temperatures and the increased proximity of gel components due to evaporation

process. EEG has a range of functional groups, including carbonyl, sulfate, and hydroxyl groups, all of which are capable of hydrogen bonding with the carboxylic and hydroxyl groups in HTOCN (Khabibullin et al., 2017, Chen et al., 2018, Pan et al., 2021, Sharif et al., 2020). In addition, at increased EEG loadings (1:2 ratio), the probability of π– π interaction between EEG nanoplatelets within the HTOCN is also enhanced, resulting in a stronger gel.

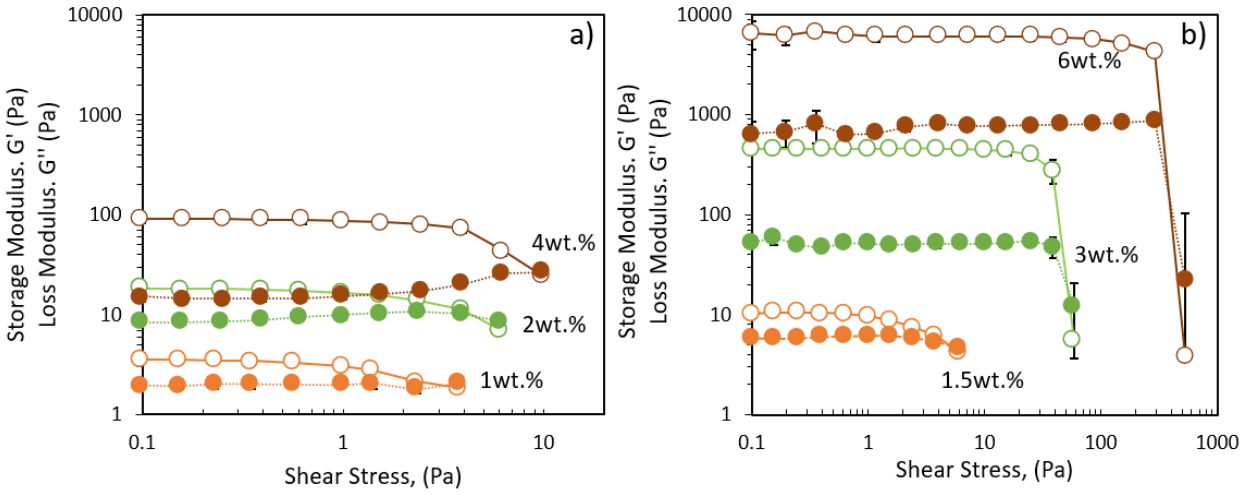

Figure 3-4 Rheological characterizations of HTOCN/EEG mixed gels at different solids content; percentage shows the amount of total solids content in the precursor gels. a) 1:1 HTOCN/EEG and b) 1:2 HTOCN/EEG.

All HTOCN/EEG gels were visualized using LSCM to gain deeper insights into the HTOCN/EEG interactions (Figure 3-5). Note that the EEG was not tagged and therefore not imaged by LSCM. However, the HTOCN network morphology can indicate the changes in the gel structure as the solids content and ratio of HTOCN/EEG were altered. It was observed that the domain sizes of the HTOCN network followed a completely different trend in HTOCN/EEG 1:1 and HTOCN/EEG 1:2 gels. The HTOCN domain size was observed to decrease with increasing solids content (increasing water evaporation percentage) in HTOCN/EEG 1:1 gels, while the opposite was true for HTOCN/EEG 1:2 gels. Since the HTOCN loading in both 1:1 and 1:2 gels remained the same,

the increasing HTOCN domains sizes with evaporation can be attributed to the packing of more EEG sheets within the HTOCN network in the case of 1:2 cryogels. The observation is consistent with the rheological signature of the precursor gels, which show approximately two orders of magnitude stronger network for the HTOCN/EEG 1:2 gel after 50 and 75 wt.% of water is evaporated, compared to 1:1 HTOCN/EEG gels with the same water evaporation amounts.

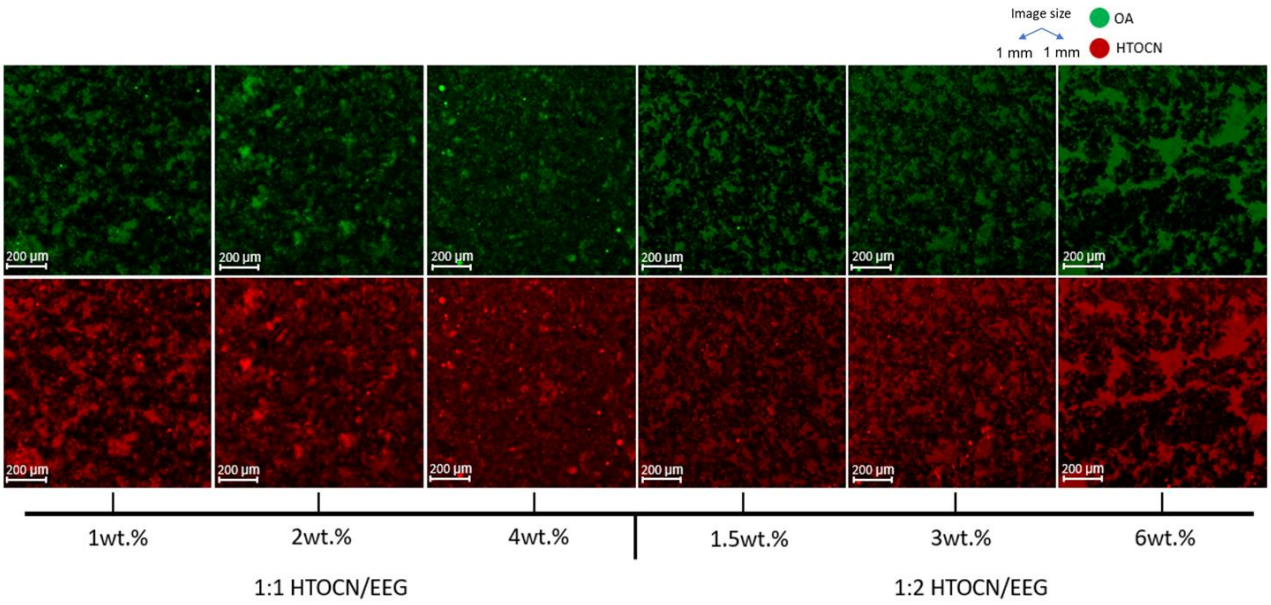

Figure 3-5 LSCM images of 1:1 HTOCN/EEG and 1:2 HTOCN/EEG as a function of water evaporation in the precursor gels; percentage shows the amount of solids content.

SEM micrographs of the freeze-dried cryogels (Figure 3-6) are consistent with the microstructure of the corresponding gels' observed via LSCM. The pore size of the 1:1 HTOCN/EEG decreased with increasing solids content (obtained by evaporation of more water from the gel precursor), while the size of the solid phase domains and the pores increased with increasing solids content for the 1:2 HTOCN/EEG cryogels. The SEM micrographs also indicate the presence of aggregates of EEG platelets, which can be held together by $\pi-\pi$ interactions or be separated by the HTCON fibers. Higher magnification images (Figure 3-6, second row) show the presence of HTOCN fibers

in the pores of the network, which are connecting EEG sheets. The SEM images also show that the wall thickness and roughness change with both solids content and EEG loading (see SI Figure S6 for additional SEM images). As seen from the images, the pore walls became thicker as whenever the EEG loading in the precursor gel was 2 wt.% or higher, indicating the presence of stacks of EEG sheets within the pore walls.

The cryogels with lower EEG loading have thinner walls, giving the cryogel flexibility (see Video S1 in SI for the flexibility of 1:1 HTOCN/EEG 1 wt.% solids content). However, with increasing EEG loading, the flexibility of the cryogel was lost (see Video S2 in SI), which further confirms that stacks of EEG nanoplates were present in the HTOCN network at higher EEG loading.

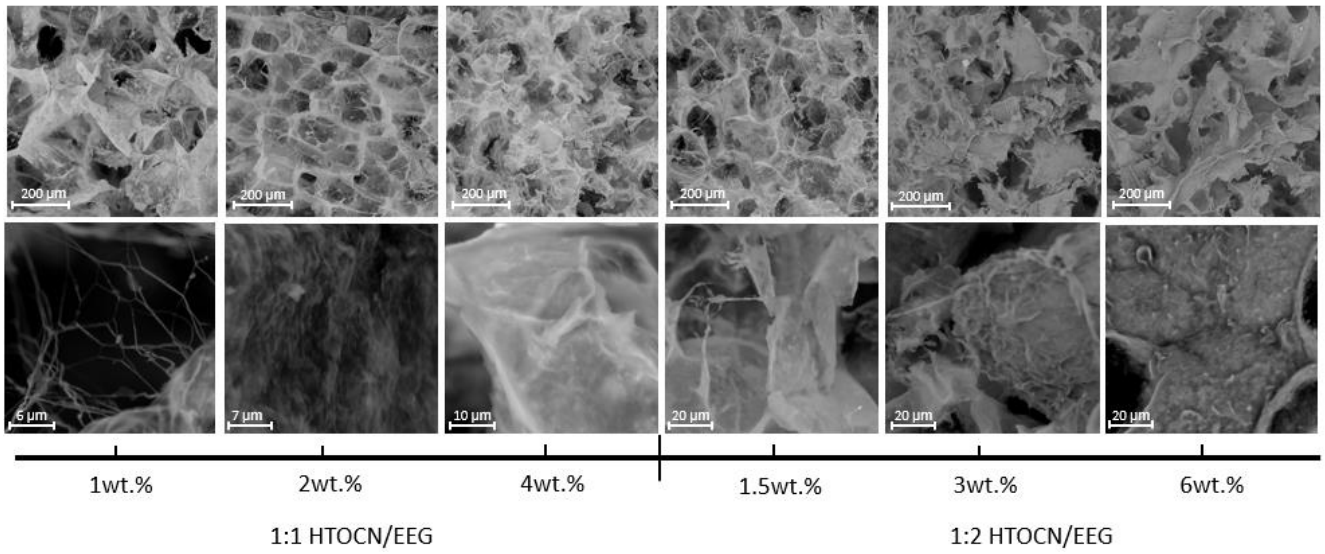

Figure 3-6 SEM images of HTOCN/EEG at different EEG loading and solids content; percentage shows the solids content by weight.

3.3.3 Adsorption isotherm

Prior to investigating cryogels', we investigated the adsorption capacity of their building blocks for the model organic contaminant, methylene blue dye. The adsorption isotherm for the HTOCN

cryogel is shown in Figure S7 and the maximum adsorption capacity was found to be 42.04 mg/g with 12.71 L/mg Langmuir constant. On the other hand, the maximum adsorption capacity of EEG nanoplatelets was 162 mg/g with Langmuir constant of 15 L/mg (reported previously (Lopez Pablos, 2021)). Figure 3-7 shows the adsorption isotherms obtained for the HTOCN/EEG cryogels at room temperature (21 ± 1 °C). The Langmuir model was fitted to the experimental data by non-linear regression, and the model parameters are summarized in Table 3-1. A notable increase in the maximum adsorption capacity for both 1:1 HTOCN/EEG and 1:2 HTOCN/EEG cryogels was observed when the solids content in their precursor gels was increased. As EEG has a much higher adsorption capacity, the higher EEG content cryogels (1:2 HTOCN/EEG) had a significantly higher maximum adsorption capacity compared to the 1:1 HTOCN/EEG cryogels, as expected.

When the solids content of the precursor gels (1:1 HTOCN/EEG cryogels) was increased from 1% to 4 wt.%, the maximum adsorption capacity increased linearly by 180% (see Figure S8). This indicates that when the solids content of the gel was increased, additional surface area is available in the resulting cryogel for the adsorption of methylene blue. The SEM and LSCM images of 1:1 HTOCN/EEG cryogels showed that precursor gels with increasing solids content led to structures with smaller pores, consistent with an increase in accessible surface area. The loadings of precursor gel components have an impact on the level of interaction between HTOCN and EEG, resulting in different amounts of accessible oxygen-containing sites, surface roughness, and specific surface area available for adsorption, thus altering the loadings can influence the adsorption performance (Hussain et al., 2018).

The adsorption isotherms of 1:2 HTOCN/EEG cryogels show that doubling the EEG loading in the precursor cryogel (no evaporation) enhances the adsorption capacity significantly by ~2.4 times compared to 1:1 HTOCN/EEG with no water evaporation. The higher adsorption capacity

of EEG particles explains the increasing adsorption capacity of 1:2 HTOCN/EEG compared to 1:1 HTOCN/EEG cryogels. However, increasing cryogel density induced by evaporating water from these precursor gels does not increase the adsorption capacity at the same rate as observed in 1:1 HTOCN/EEG cryogels. It is apparent that with the increase in solids content, the loss of accessible surface area due to particle aggregation occurs. Consequently, an increase in the solids content from 1.5 to 6 wt.% in the 1:2 HTOCN/EEG precursor gel results in only a 70% rise in the adsorption capacity of the cryogel, compared to an increase of 180% observed when the solids content of 1:1 HTOCN/EEG precursor gel was increased from 1 to 4 wt.%. These results are consistent with the SEM images, which indicated the presence of stacked EEG sheets, thus having less accessible adsorption sites.

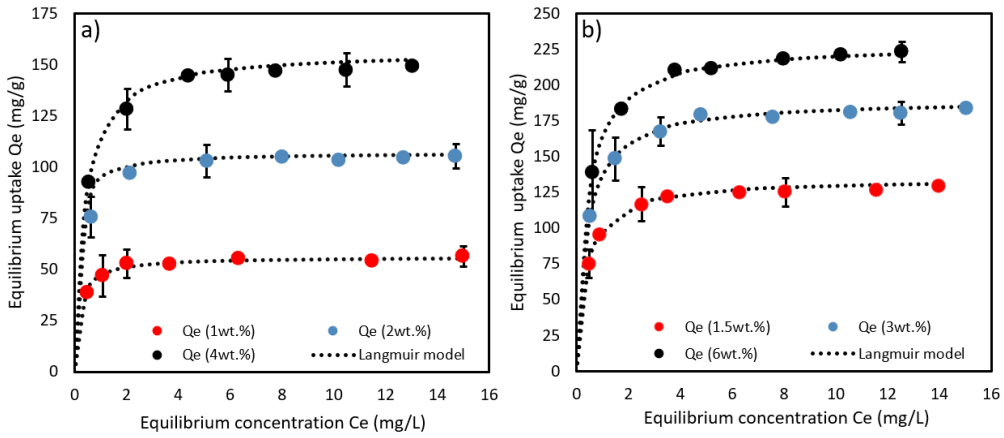

Figure 3-7 Adsorption isotherm of a) 1:1 HTOCN/EEG and b) 1:2 HTOCN/EEG cryogels prepared at different solids content, percentages show the solid weight percent. Experimental conditions: mixing time 24 hours, room temperature, and pH 7.

Table 3-3 Estimated Langmuir adsorption isotherm parameters for HTOCN/EEG with different EEG loading and solids content.

Cryogel	Solids content	Q_m (mg/g)	K_L (L/mg)	χ^2
1:1 HTOCN/EEG	1 wt.%	56.01	5.08	0.17
	2 wt.%	107.08	3.95	0.80
	4 wt.%	156.63	2.68	0.39
1:2 HTOCN/ EEG	1.5 wt.%	134.41	2.63	0.27
	3 wt.%	189.81	2.53	0.29
	6 wt.%	228.90	2.45	0.10

3.3.4 Electrochemical regeneration

Following the adsorption experiments, HTOCN/EEG cryogels were exposed to anodic oxidation (see Figure S4 for the setup). The regeneration efficiency was evaluated for all the investigated cryogels over five adsorption and electrochemical regeneration cycles (Figure 3-8a).

All six cryogels were successfully regenerated, and exhibited an increase in the maximum adsorption capacities of around 10-20% of the initial capacity after the fifth cycle. The increasing regeneration efficiency could be ascribed to roughening of the adsorbent surface and pore walls, oxidation of EEG along with the contaminant, and/or creating more accessible pores, thus creating more adsorption sites (Nkrumah-Amoako et al., 2014, Asghar et al., 2012, Sharif and Roberts, 2020). The electrochemical regeneration in the presence of Na_2SO_4 electrolyte may alter the surface chemistry, forming active adsorption sites and increasing the surface area by roughening the surface and creating small pores. The SEM images (Figure S9) of adsorbents after the adsorption/regeneration cycles confirmed changes on the surface due to electrochemical

regeneration. The surface of cryogels became rougher, and small pores are created, which increase the specific surface area and create more adsorption sites.

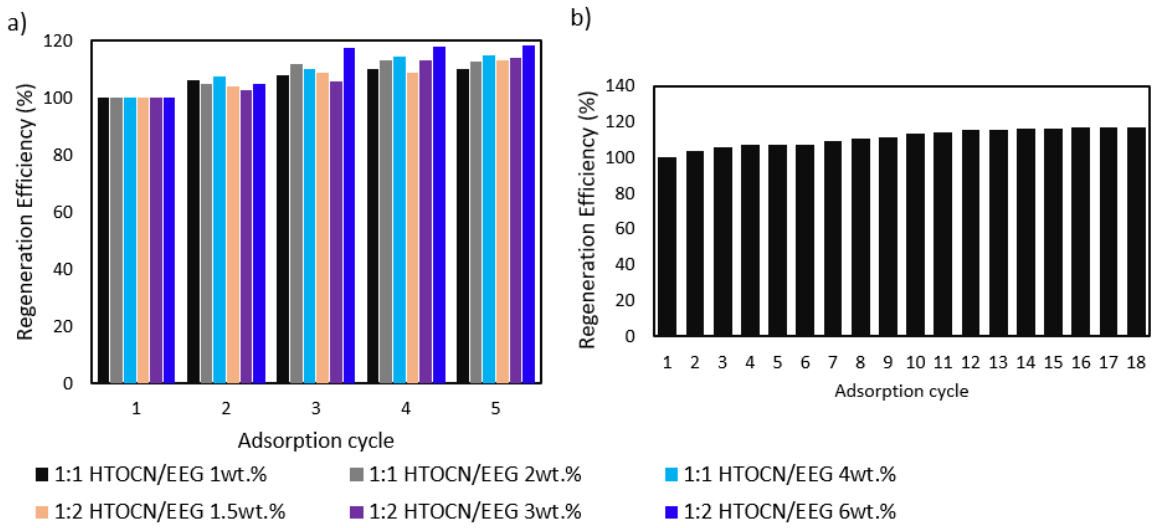

Figure 3-8 Regeneration efficiency over adsorption and electrochemical regeneration cycles for a) 5 cycles for 1:1 and 1:2 HTOCN/EEG, b) 18 cycles for 1:1 HTOCN/EEG 1 wt.% solids content cryogels.

The adsorption of methylene blue on EEG nanoplatelets prepared by the same method, and their anodic electrochemical regeneration, has been studied previously (Lopez Pablos, 2021). It was reported that the adsorption capacity decreased after a few cycles of electrochemical regeneration cycles, and this was attributed to mass loss during filtration or regeneration. Another study performed on commercial graphene (Sharif and Roberts, 2020), showed an increase in the adsorption capacity to 110% after the first adsorption cycle, reaching approximately 130% after the third cycle, and decreased slightly after the third cycle (125%). The authors attributed the increase in the maximum adsorption capacity to the increased surface area of the adsorbent and/or adding more functional groups due to surface oxidation during electrochemical regeneration. The oxidation results in adding more oxygen-containing functional groups on graphene sheets and

increases the surface area. Evidence for corrosion of the graphene was supported by approximately 30% of the initial mass lost at the end of the fifth cycle (although this may be due to the loss of regenerated nanoparticles during filtration), and the presence of brown color in the solution due to the corroded graphene sheets (Sharif and Roberts, 2020, Sharif et al., 2017).

The derived HTOCN/EEG cryogels offer several advantages, such as it requires no filtration step to separate the cryogels from the treated water, and it serves as a conductive collector (adsorbent) attached to the anode, which improves the overall adsorption and electrochemical regeneration efficiency. Besides that, we have not observed any change in the color nor mass loss after five adsorption/regeneration cycles indicating resistance to corrosion and high structural integrity of all cryogels. The resistance to corrosion could be induced by the presence of the HTOCN network. To further confirm our hypothesis, we carried out 18 adsorption-electrochemical regeneration cycles (Figure 3-8 b) using the lowest density 1:1 HTOCN/EEG cryogel. The adsorption was found to increase slightly over 18 cycles and leveled off at around 120% after 10 cycles. The cryogel was then freeze-dried, and its mass was measured; no mass loss was observed after 18 adsorption-regeneration cycles, which supports the hypothesis that HTOCN protects the graphene surface from corrosion, resulting in structurally sound and chemically stable cryogels.

The successful electrochemical regeneration of the 1:1 HTOCN/EEG 1 wt.% was also assessed by LSCM imaging after adsorption and after the subsequent electrochemical regeneration. MB dye is autofluorescent (Hernandez-Martínez et al., 2018), and therefore, the fluorescence intensity of MB is associated with the amount of adsorbed dye on the cryogel's surface. As expected, the MB intensity was high after adsorption, and it disappeared after the electrochemical regeneration due to the oxidation of MB dye adsorbed on the cryogel (see Figure S10 in SI).

To ensure that passing a low current through the cryogel is responsible for MB oxidation process rather than desorption of MB in the presence of the electrolyte solution, a control experiment was carried out for the 1:1 HTOCN/EEG 1 wt.% solids content with no current passing through the cryogel during the regeneration cycle. The following adsorption uptake declined by ~ 60%, confirming the necessity of electrochemical regeneration to oxidize the adsorbed dye and regenerate the cryogels (Figure S11 in SI).

3.4 Conclusions

HTOCN/EEG cryogels were successfully fabricated using a simple mixing/freeze drying method and used for the adsorption and electrochemical oxidation of methylene blue organic dye. The systematic investigation of the precursor gels provided microscopic insights into the interactions between HTOCN and EEG as a function of HTONC/EEG ratio and total solids content by connecting particle network distribution to the macroscopic flow behavior of the resulting gel. We show that the enhancement of network strengths originates from HTOCN/EEG interactions at low EEG loadings while at high loadings of EEG in HTOCN/EEG 1:2 gels, the contribution of $\pi-\pi$ interactions between EEG nanoplatelets is evident. The quantitative analysis of the adsorption capacities of the corresponding cryogels is in agreement with this finding; increasing the EEG loading beyond 2 wt.% in the precursor gel results in loss of accessibility of adsorption sites in the derived cryogel due to more pronounced EEG aggregation. Similarly, cryogel's flexibility is directly influenced by the level of EEG aggregation. It was found that that cryogels can be electrochemically regenerated, withstanding up to 18 adsorption-electrochemical regeneration cycles with 10-20% increase in adsorption capacity and no detectable mass loss. The extensive characterization of the precursor gels and the corresponding cryogels demonstrates the importance of coupling the two in the design of cryogels for an application of interest. Although several

parameters were not addressed in this work (such as pH and freezing rates), our findings provide a significant step towards designing cryogels with tunable properties; thus, it could serve as a platform for different applications (e.g. pressure sensors, batteries, electrodes, etc.).

Chapter 4

Conclusion and future recommendations

4.1 Conclusion

This thesis provides a systematic approach to deriving biodegradable HTOCN/EEG cryogels that exhibit long-term stability during multiple electrochemical regeneration cycles. The following conclusions were made from this work:

- Oleic acid can successfully hydrophobize TOCN at a pH of ~ 6.85, which was confirmed by the FTIR measurements. According to the rheological measurements, the addition of OA increases the TOCN gel's strength until its loading reaches 5 wt.% (the optimum loading) before the strength decreases at higher OA loadings. The reduction in the strength was found to be due to OA droplets coalescence, confirmed by LSCM imaging.
- The initial solids content and EEG loadings impact the properties of HTOCN/EEG mixed gels. The 1:2 HTOCN/EEG were found to form a stronger network than 1:1 HTOCN/EEG when exposed to more prolonged mixing, indicating that higher EEG loadings contribute towards creating stronger gels through $\pi-\pi$ interaction between EEG nanoplatelets within the HTOCN at high solid contents (50 and 75 wt.% water evaporation).
- LSCM indicates that increasing solids content at different HTOCN/EEG ratios changes the gel structure in two trends; Smaller domains can be obtained with increasing solids content in 1:1 HTOCN/EEG, while the opposite is true for 1:2 HTOCN/EEG gels due to the orientation of EEG sheets within the HTOCN network in which higher EEG loadings gives more packed networks and less flexible cryogels. SEM images show that at higher EEG loadings (1:2 ratio), the roughness and wall thickness of cryogels pore network increased, driven by EEG aggregations within the HTOCN network.

- The adsorption capacity of cryogels increased by increasing solids content for both 1:1 and 1:2 HTOCN/EEG cryogels. The enhancement in the adsorption capacity was higher in 1:1 HTOCN/EEG cryogels (180% compared to 70% for 1:2 cryogels, when evaporating 75 wt.% of the water in the gels). SEM images indicated the presence of stacked EEG sheets in 1:2 HTOCN/EEG, thus loss of accessible surface area for adsorption on methylene blue.
- The cryogels were successfully employed for multiple cycles of adsorption of methylene blue organic dye and consequent electrochemical regeneration of cryogels. All cryogels can be regenerated with an increased maximum adsorption capacity by 10-20% of the initial capacity after the fifth cycle. The increase in the adsorption capacity can be attributed to the roughening of the adsorbent surface and pore walls induced by oxidation of EEG (evident from SEM images after regeneration), and/or creating more accessible pores and adsorption sites during the electrochemical regeneration.
- Eighteen adsorption-electrochemical regeneration cycles were performed using 1:1 HTOCN/EEG (1 wt.% solid content) cryogel. The adsorption leveled off at around 120% after the 10^{th} cycle confirming the long-term stability of the derived cryogels. Furthermore, LSCM images of cryogels after electrochemical regeneration showed that the intensity of MB disappeared, confirming the successful regeneration of the cryogel.
- The electrochemical regeneration was performed for one cycle with no current to ensure that the current is responsible for the regeneration of cryogels rather than the desorption of MB in the electrolyte solution. The following adsorption uptake dropped by ~ 60%, confirming the necessity of electric current for the regeneration of cryogels and oxidation of MB.

4.2 Future recommendations

Cryogels properties depend on too many other factors that were not addressed in this work. Understanding these factors will contribute towards widening the use of HTOCN/EEG for other applications. The factors and future recommendations are listed below:

- This work mainly focused on understanding and synthesizing cryogels that have long-term stability under electrochemical regeneration conditions. The analysis of the treated water and the possibility of formation of breakdown products that may be released into the treated water was not investigated in this study, and further work is needed to explore this aspect.
- pH of the gels. This work was done at a pH of around seven, and exploring different pHs' can alter the interactions between the component. The pH mainly impacts the deprotonation of the oxygen-containing functional groups on TOCN, OA, and EEG, adding additional room for modifications and structure enhancement. Furthermore, adjusting the pH alters the interactions with the ice crystals giving different morphologies, hydrophobicity, and final properties.
- HTOCN/EEG cryogels, prepared at different EEG loadings and solid contents, were evaluated. The freezing velocity and directionality were not controlled, thus using unidirectional freezing and exploring the effect of freezing velocity, which plays an essential role on the final properties of the cryogel can give different morphologies.
- The ice crystals growth determines the pore morphology. This work studied the morphology of cryogels after the freeze-drying; therefore, the use of Cryo-SEM to probe the effect of loadings and solids content on the ice crystals' growth and the orientation of

HTOCN and EEG during the freezing may give further insights into the structuring mechanism.

- Two different ratios of HTOCN/EEG were investigated 1:1 and 1:2, the further increase of EEG loading would enhance the conductivity of the cryogel, thus, widening the applications where it can be used, such as sensors and electrodes.
- The adsorption and electrochemical regeneration were done in batch modes. Testing the cryogels in a flow-through setup while current is applied to allow the adsorption and electrochemical oxidation of organics to occur continuously on larger scales would be beneficial for scale-up purposes.
- The cryogel has conductive EEG, and the ones with low solid contents showed good flexibility. They can return and recover to their original shape upon exposing them to pressure. Therefore, they might fit the pressure sensors applications.
- Oxygen evolution side reaction was observed on the cryogels surfaces during the electrochemical regeneration, which might have reduced the regeneration efficiency and increased the time needed to regenerate the cryogels by trapping oxygen within the cryogel. Switching the cathode and anode for a short period of time would remove the build-up oxygen bubbles on and within the cryogel, thus enhancing regeneration efficiency. Furthermore, the time needed to regenerate the cryogels fully is required to reduce the unnecessary exposure of the cryogel to the current and reduce energy consumption.
- EEG particles were first synthesized using electrochemical exfoliation of graphene in the presence of ammonium sulfate electrolyte before drying and re-dispersing the EEG particles in water. The EEG dispersion was then mixed with HTOCN to prepare the cryogels. The electrochemical exfoliation of graphene in the presence of HTOCN might

produce cryogels with entirely different properties, as well as reduce the time needed and cost for making these materials by turning them into a more straightforward one-step process.

Appendix A

Supporting information

Biodegradable Cryogels for Adsorption and Electrochemical Oxidation of Dissolved Organic Dyes

The fluorophore labeling of TOCN was done by mixing 50 mL of 1.1 wt.% TOCN with 20 mg Rhodamine B Isothiocyanate dye and NaOH. NaOH was added until its final concentration is 0.1 M. The tagged TOCN dispersion (TOCN-RITC) was mixed for three days at 300 rpm. After that, the dispersion was centrifuged, and the lower denser portion of TOCN was dialyzed against DI until the tagged TOCN's pH is 7 and no free dye in the DI. The concentration of TOCN was then calculated and readjusted to 1 wt.% for imaging.

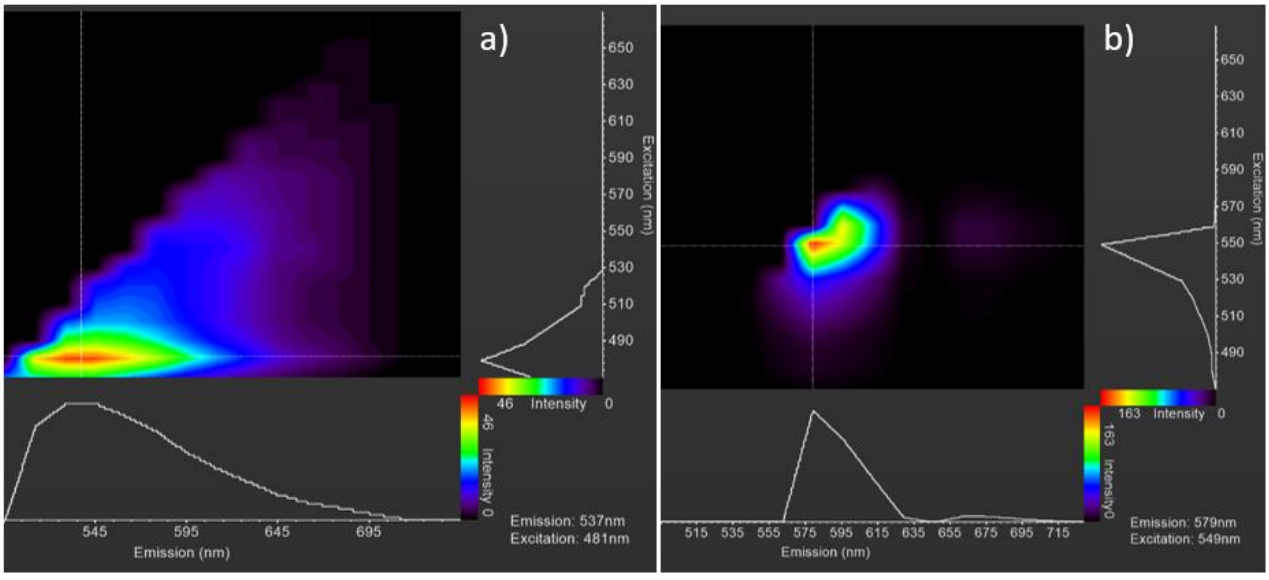

Figure S1 Excitation/Emission fluorescence scan from 470-780 nm of a) OA and b) TOCN-RITC.

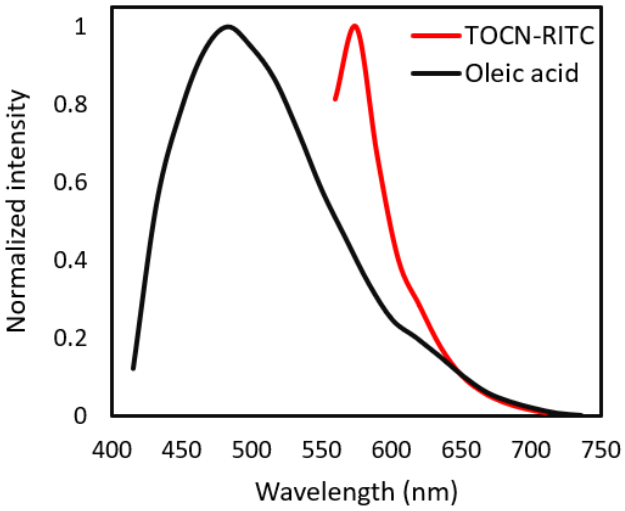

Figure S2 Emission spectra of OA and tagged TOCN, excited with 405 nm and 550 nm laser lines, respectively. There was no overlapping in the OA recorded emission (420 – 520 nm), while OA overlaps with the tagged TOCN (565 – 620 nm).

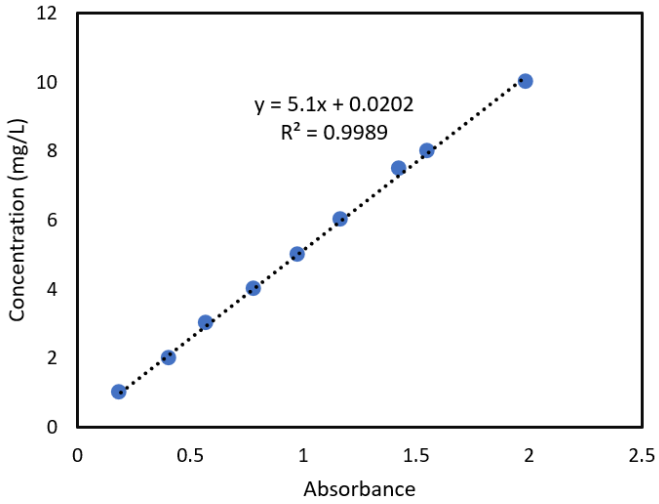

Figure S3 Calibration curve of MB organic dye at 664 nm wavelength and pH 7.

The Langmuir adsorption model was used to fit the experimental data. The model assumes a homogenous adsorbent surface, where molecules get adsorbed onto a monolayer surface with equal adsorption energy for all binding sites and negligible attraction between the adsorbed molecules. The non-linear Langmuir equation used for the modeling part to fit the experimental data is shown below (Langmuir, 1918, Abuhatab et al., 2019):

$$Q_e = \frac{Q_m K_L C_e}{1 + K_L C_e}$$

where Q_e is the adsorption capacity at equilibrium (mg/g), K_L is the Langmuir constant (L/mg), C_e is the equilibrium concentration of MB (mg/L), Q_m is the maximum capacity of the adsorbent (mg/g).

The following mass balance equation was used to calculate the experimental adsorption uptake at equilibrium (Abuhatab et al., 2019):

$$Q_e = \frac{V(C_o - C_e)}{m}$$

where V is the volume of solution containing MB (L), C_e is the equilibrium concentration of MB (mg/L), C_o is the initial concentration of MB (mg/L), and m is the mass of cryogel adsorbent (g).

The goodness of the Langmuir model was evaluated using the non-linear Chi-square (χ^2) shown below (Abuhatab et al., 2019):

$$\chi^2 = \sum \frac{(Q_e - Q_{e(model)})^2}{Q_{e(model)}}$$

where Qe and $Q_{e(model)}$ are the equilibrium uptakes calculated experimentally and by model fitting, respectively.

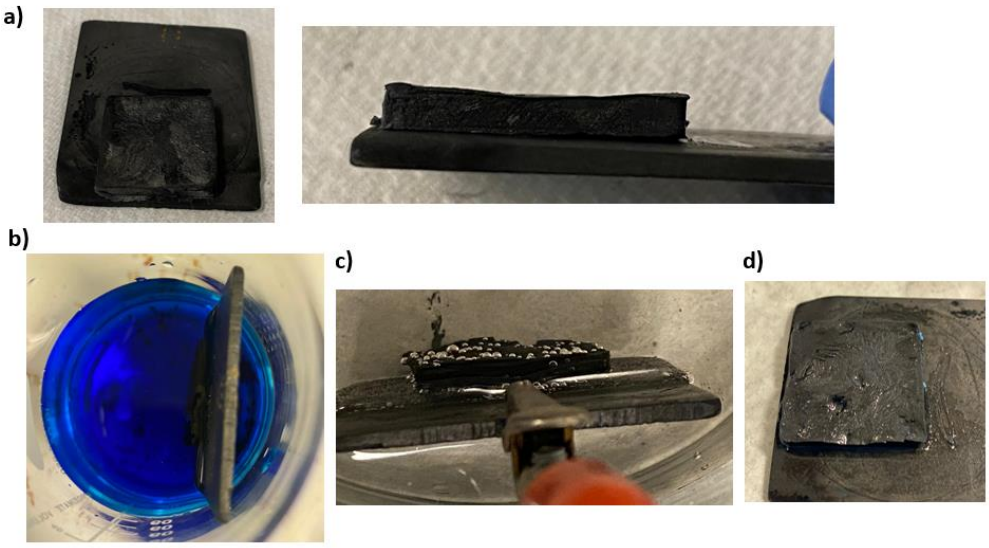

Figure S4 1:1 HTOCN/EEG 1 wt.% solid content cryogel images, foam dimensions: (23mm×23mm×2mm) a) before the adsorption and electrochemical regeneration, b) during adsorption, c) during electrochemical regeneration, d) after regeneration.

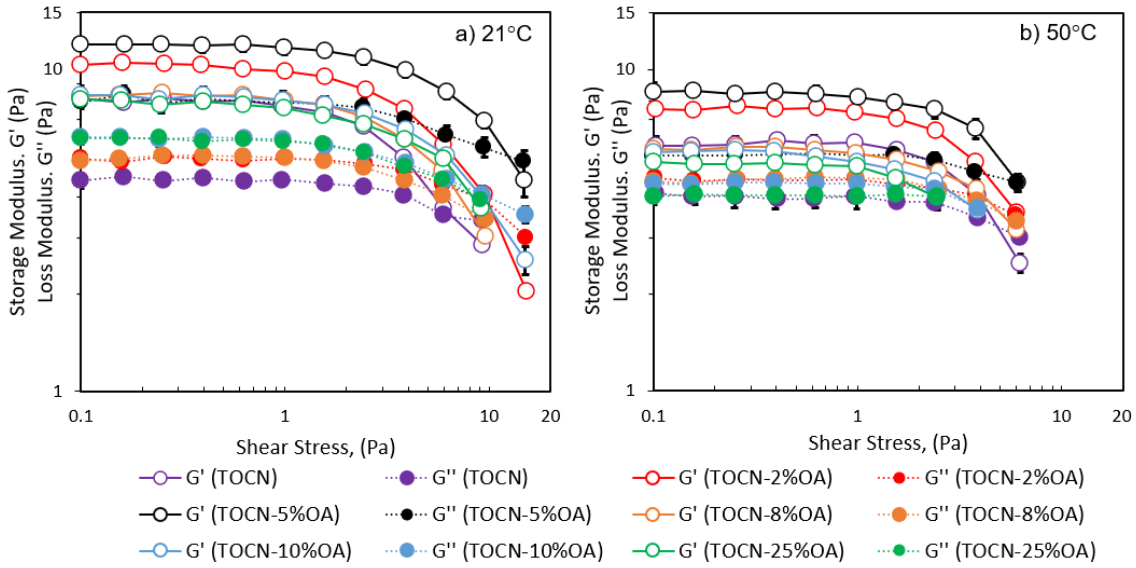

Figure S5 Additional rheological measurements of HTOCN mixed gels at different OA loadings; percentage shows the amount of OA by weight. a) Shear stress sweep at 21 ± 1 °C and b) shear stress sweep at 50 °C.

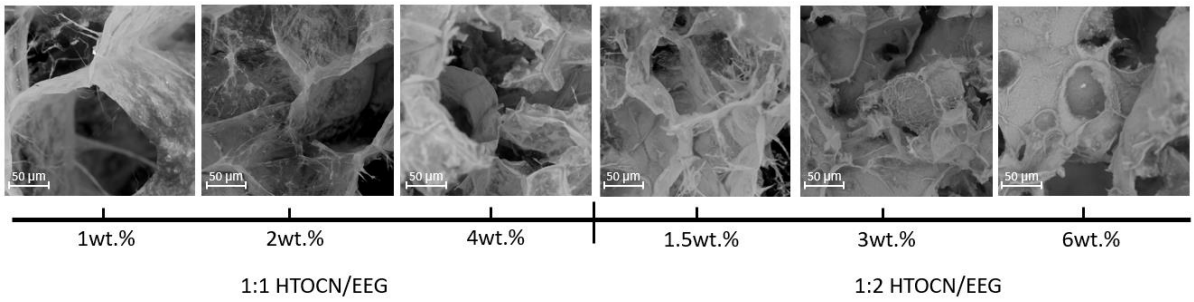

Figure S6 Additional SEM images of HTOCN/EEG cryogels using different magnification.

1 1 HTOCN EEG 1wt.%.mp4

Video S1 1:1 HTOCN/EEG 1 wt.% cryogel immersed in a solution containing methylene blue organic dye.

1 2 HTOCN EEG 6wt.%.mp4

Video S2 1:2 HTOCN/EEG 6 wt.% cryogel immersed in a solution containing methylene blue organic dye.

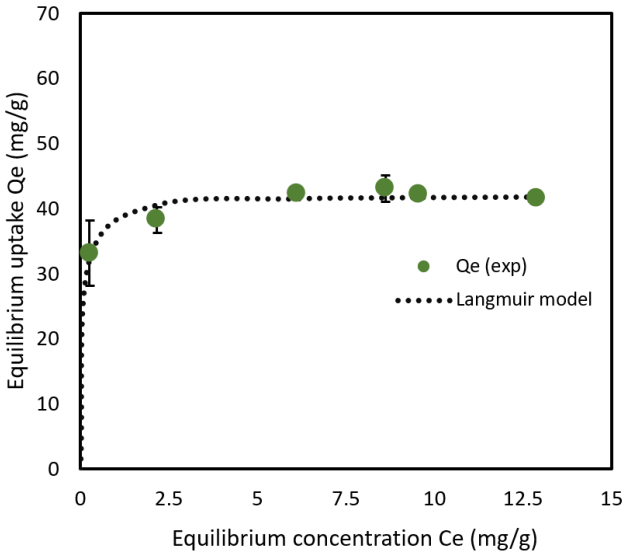

Figure S7 Adsorption isotherm of HTOCN cryogel. Experimental conditions: mixing time 24 hours, room temperature, and pH 7. The solid dashed line is the Langmuir model, while the data points are the experimental data. The estimated maximum adsorption capacity and Langmuir constant were 42.04 (mg/g) and 12.71 (L/mg), respectively, with an error value of 0.227.

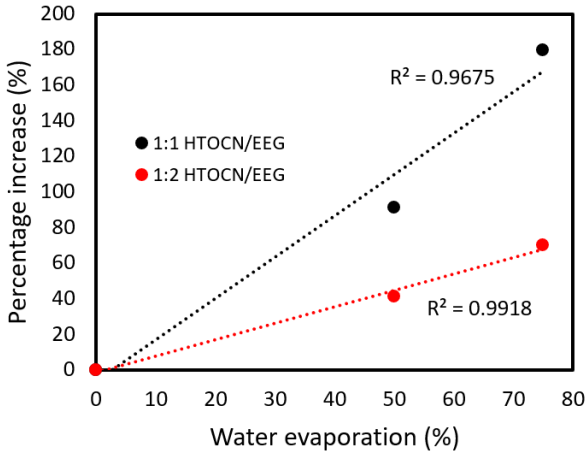

Figure S8 Effect of water evaporation on the adsorption capacity enhancement in1:1 HTOCN/EEG, compared to 1:2 HTOCN/EEG cryogels.

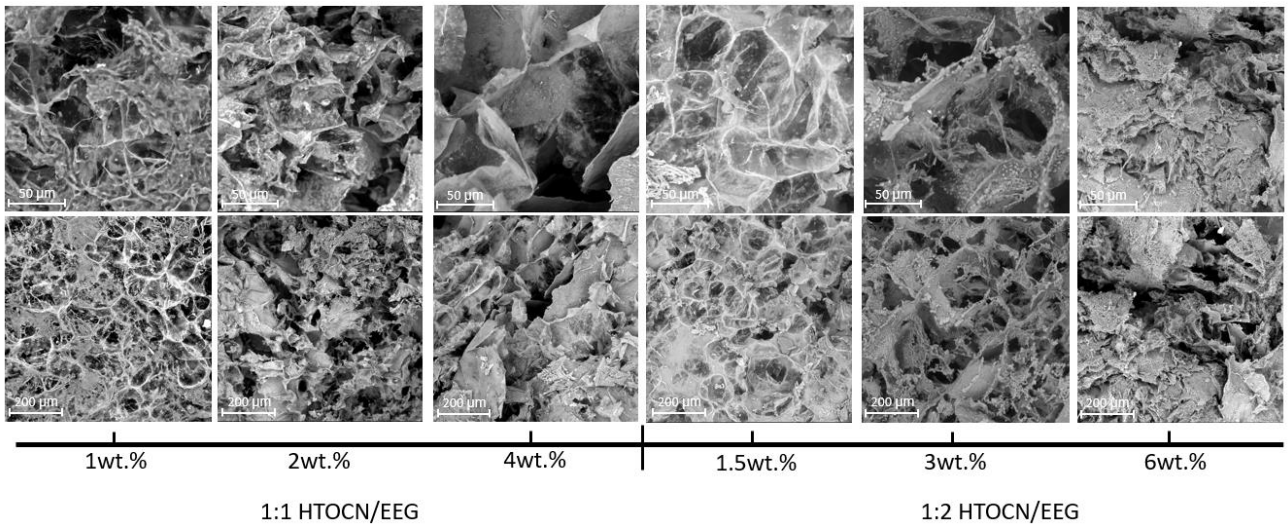

Figure S9 SEM images of the regenerated HTOCN/EEG cryogels. 1:1 HTOCN/EEG 1 wt.% solids content images were taken after 18 adsorption-electrochemical regeneration cycles, while all other foams were imaged after 5 cycles.

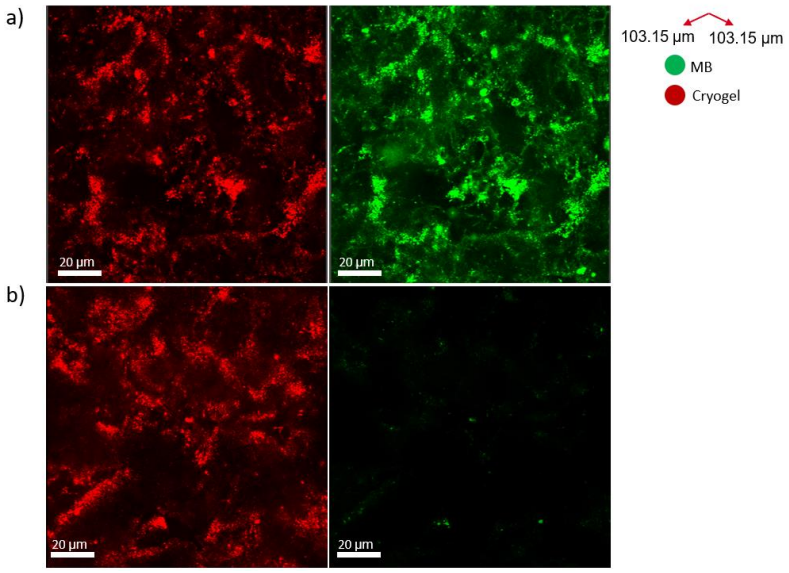

Figure S10 LSCM images of 1:1 HTOCN/EEG 1 wt.% solid content cryogel surface a) after adsorption and b) after electrochemical regeneration. Cryogel was imaged in reflectance mode at 760 nm, while MB was imaged using fluorescence mode (excited at 650 nm and emitted from 665-

720 nm (Hernandez-Martínez et al., 2018)). Imaging setup: 63x magnification objective, 1024×1024 image format, 100 nm pixel size, 0.8 AU pinhole, and 400 Hz scanning speed.

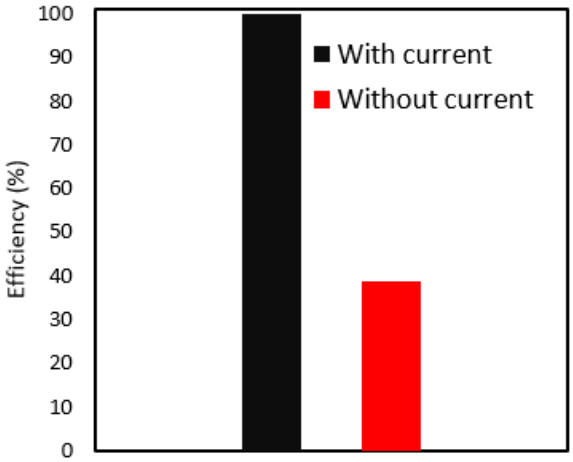

Figure S11 Control experiment for the regeneration efficiency of 1:1 HTOCN/EEG 1 wt.% solid content with and without current passing through the cryogel.

References

Abdul Khalil, H. P. S., Davoudpour, Y., Islam, M. N., Mustapha, A., Sudesh, K., Dungani, R. and Jawaid, M. 2014. Production and modification of nanofibrillated cellulose using various mechanical processes: A review. *Carbohydrate Polymers,* 99**,** 649-665.

Abou-Taleb, E. M., Hellal, M. S. and Kamal, K. H. 2021. Electro-oxidation of phenol in petroleum wastewater using a novel pilot-scale electrochemical cell with graphite and stainless-steel electrodes. *Water and Environment Journal,* 35**,** 259-268.

Abuhatab, S., El-Qanni, A., Marei, N. N., Hmoudah, M. and El-Hamouz, A. 2019. Sustainable competitive adsorption of methylene blue and acid red 88 from synthetic wastewater using NiO and/or MgO silicate based nanosorbcats: experimental and computational modeling studies. *RSC Advances,* 9**,** 35483-35498.

Ahmad, A. L., Jawad, Z. A., Low, S. C. and Zein, S. H. S. 2014. A cellulose acetate/multi-walled carbon nanotube mixed matrix membrane for CO2/N2 separation. *Journal of Membrane Science,* 451**,** 55-66.

Al-Ahmed, Z. A., Hassan, A. A., El-Khouly, S. M. and El-Shafey, S. E. 2020. TEMPO-oxidized cellulose nanofibers/TiO2 nanocomposite as new adsorbent for Brilliant Blue dye removal. *Polymer Bulletin,* 77**,** 6213-6226.

Almazán-Almazán, M. C., Léonard, A., López-Garzón, J., Abdullah, J., Marchot, P. and Blacher, S. 2009. 3D characterisation of the structure of activated carbon packed beds using X-ray microtomography *3rd International Workshop on Process Tomography*

Amaral-Labat, G., Szczurek, A., Fierro, V., Stein, N., Boulanger, C., Pizzi, A. and Celzard, A. 2012. Pore structure and electrochemical performances of tannin-based carbon cryogels. *Biomass and Bioenergy,* 39**,** 274-282.

Andrés García, E., Agulló-Barceló, M., Bond, P., Keller, J., Gernjak, W. and Radjenovic, J. 2018. Hybrid electrochemical-granular activated carbon system for the treatment of greywater. *Chemical Engineering Journal,* 352**,** 405-411.

Anglada, Á., Urtiaga, A. and Ortiz, I. 2009. Contributions of electrochemical oxidation to waste-water treatment: fundamentals and review of applications. *Journal of Chemical Technology & Biotechnology,* 84**,** 1747-1755.

Anjum, M., Miandad, R., Waqas, M., Gehany, F. and Barakat, M. A. 2019. Remediation of wastewater using various nano-materials. *Arabian Journal of Chemistry,* 12**,** 4897-4919.

Asghar, H. M. A., Roberts, E. P. L., Hussain, S. N., Campen, A. K. and Brown, N. W. 2012. Wastewater treatment by adsorption with electrochemical regeneration using graphite-based adsorbents. *Journal of Applied Electrochemistry,* 42**,** 797-807.

Ayawei, N., Ebelegi, A. N. and Wankasi, D. 2017. Modelling and Interpretation of Adsorption Isotherms. *Journal of Chemistry,* 2017**,** 3039817.

Bagreev, A., Rahman, H. and Bandosz, T. J. 2001. Thermal regeneration of a spent activated carbon previously used as hydrogen sulfide adsorbent. *Carbon,* 39**,** 1319-1326.

Baimenov, A., Berillo, D. A., Poulopoulos, S. G. and Inglezakis, V. J. 2020. A review of cryogels synthesis, characterization and applications on the removal of heavy metals from aqueous solutions. *Advances in Colloid and Interface Science,* 276**,** 102088.

Benkaddour, A., Journoux-Lapp, C., Jradi, K., Robert, S. and Daneault, C. 2014. Study of the hydrophobization of TEMPO-oxidized cellulose gel through two routes: amidation and esterification process. *Journal of Materials Science,* 49**,** 2832-2843.

Bonenfant, D., Niquette, P., Mimeault, M. and Hausler, R. 2010. Adsorption and recovery of nonylphenol ethoxylate on a crosslinked β-cyclodextrin-carboxymethylcellulose polymer. *Water Science and Technology,* 61**,** 2293-2301.

Bruns, J., McBride-Gagyi, S. and Zustiak, S. P. 2018. Injectable and Cell-Adhesive Polyethylene Glycol Cryogel Scaffolds: Independent Control of Cryogel Microstructure and Composition. *Macromolecular Materials and Engineering,* 303**,** 1800298.

Buchtová, N., Pradille, C., Bouvard, J.-L. and Budtova, T. 2019. Mechanical properties of cellulose aerogels and cryogels. *Soft Matter,* 15**,** 7901-7908.

Canencia, F., Darder, M., Aranda, P., Fernandes, F. M., Gouveia, R. F. and Ruiz-Hitzky, E. 2017. Conducting macroporous carbon foams derived from microwave-generated caramel/silica gel intermediates. *Journal of Materials Science,* 52**,** 11269-11281.

Carpenter, A. W., de Lannoy, C.-F. and Wiesner, M. R. 2015. Cellulose Nanomaterials in Water Treatment Technologies. *Environmental Science & Technology,* 49**,** 5277-5287.

Carvalho, B. M. A., Da Silva, S. L., Da Silva, L. H. M., Minim, V. P. R., Da Silva, M. C. H., Carvalho, L. M. and Minim, L. A. 2014. Cryogel Poly(acrylamide): Synthesis, Structure and Applications. *Separation & Purification Reviews,* 43**,** 241-262.

Cervin, N. T., Aulin, C., Larsson, P. T. and Wågberg, L. 2012. Ultra porous nanocellulose aerogels as separation medium for mixtures of oil/water liquids. *Cellulose,* 19**,** 401-410.

Chandrasekaran, S., Cerón, M. R. and Worsley, M. A. 2021. CHAPTER 1 Engineering the Architecture of 3D Graphene-based Macrostructures. *Graphene-based 3D Macrostructures for Clean Energy and Environmental Applications.* The Royal Society of Chemistry.

Chen, G., Zhang, B. and Zhao, J. 2015. Dispersion Process and Effect of Oleic Acid on Properties of Cellulose Sulfate- Oleic Acid Composite Film. *Materials,* 8**,** 2346-2360.

Chen, Y., Pötschke, P., Pionteck, J., Voit, B. and Qi, H. 2018. Smart cellulose/graphene composites fabricated by in situ chemical reduction of graphene oxide for multiple sensing applications. *Journal of Materials Chemistry A,* 6**,** 7777-7785.

Ciolacu, D., Rudaz, C., Vasilescu, M. and Budtova, T. 2016. Physically and chemically cross-linked cellulose cryogels: Structure, properties and application for controlled release. *Carbohydrate Polymers,* 151**,** 392-400.

Connors, S., Lanza, R. and Sirocki, A. 2013. *Removal of Ibuprofen from Drinking Water using Adsorption.* Removal of Ibuprofen from Drinking Water using Adsorption.

Corte, A. E. 1963. Particle Sorting by Repeated Freezing and Thawing. *Science,* 142**,** 499.

Cristina Oliveira Neves, I., Aparecida Rodrigues, A., Teixeira Valentim, T., Cristina Freitas de Oliveira Meira, A., Henrique Silva, S., Ayra Alcântara Veríssimo, L. and Vilela de Resende, J. 2020. Amino acid-based hydrophobic affinity cryogel for protein purification from ora-pro-nobis (Pereskia aculeata Miller) leaves. *Journal of Chromatography B,* 1161**,** 122435.

Davis, M. E. 2002. Ordered porous materials for emerging applications. *Nature,* 417**,** 813-821.

De Gisi, S., Lofrano, G., Grassi, M. and Notarnicola, M. 2016. Characteristics and adsorption capacities of low-cost sorbents for wastewater treatment: A review. *Sustainable Materials and Technologies,* 9**,** 10-40.

Demirci, S. and Sahiner, N. 2020. The Use of Conductive Polymers Embedded Macro Porous Pei and Ionic Liquid Form of Pei Cryogels for Potential Conductometric Sensor Application to CO2. *Journal of Composites Science,* 4**,** 27.

Deng, F., Luo, X.-B., Ding, L. and Luo, S.-L. 2019. 5 - Application of Nanomaterials and Nanotechnology in the Reutilization of Metal Ion From Wastewater. *In:* Luo, X.andDeng, F. (eds.) *Nanomaterials for the Removal of Pollutants and Resource Reutilization.* Elsevier.

Deng, Z., Guo, Y., Ma, P. X. and Guo, B. 2018. Rapid thermal responsive conductive hybrid cryogels with shape memory properties, photothermal properties and pressure dependent conductivity. *Journal of Colloid and Interface Science,* 526**,** 281-294.

Deville, S., Maire, E., Lasalle, A., Bogner, A., Gauthier, C., Leloup, J. and Guizard, C. 2010. Influence of Particle Size on Ice Nucleation and Growth During the Ice-Templating Process. *Journal of the American Ceramic Society,* 93**,** 2507-2510.

Deville, S., Saiz, E. and Tomsia, A. P. 2006. Freeze casting of hydroxyapatite scaffolds for bone tissue engineering. *Biomaterials,* 27**,** 5480-5489.

Deville, S., Saiz, E. and Tomsia, A. P. 2007. Ice-templated porous alumina structures. *Acta Materialia,* 55**,** 1965-1974.

Deville, S., Viazzi, C., Leloup, J., Lasalle, A., Guizard, C., Maire, E., Adrien, J. and Gremillard, L. 2011. Ice Shaping Properties, Similar to That of Antifreeze Proteins, of a Zirconium Acetate Complex. *PLOS ONE,* 6**,** e26474.

Dilamian, M. and Noroozi, B. 2021. Rice straw agri-waste for water pollutant adsorption: Relevant mesoporous super hydrophobic cellulose aerogel. *Carbohydrate Polymers,* 251**,** 117016.

Dobritoiu, R. and Patachia, S. 2013. A study of dyes sorption on biobased cryogels. *Applied Surface Science,* 285**,** 56-64.

Doke, K. M. and Khan, E. M. 2013. Adsorption thermodynamics to clean up wastewater; critical review. *Reviews In Environmental Science And Biotechnology,* 12**,** 25-44.

El Gamal, M., Mousa, H. A., El-Naas, M. H., Zacharia, R. and Judd, S. 2018. Bio-regeneration of activated carbon: A comprehensive review. *Separation and Purification Technology,* 197**,** 345-359.

Elshorbagy, W. and Chowdhury, R. K. 2013. *Water treatment* IntechOpen.

Estevez, L., Barpaga, D., Zheng, J., Sabale, S., Patel, R. L., Zhang, J.-G., McGrail, B. P. and Motkuri, R. K. 2018. Hierarchically Porous Carbon Materials for CO2 Capture: The Role of Pore Structure. *Industrial & Engineering Chemistry Research,* 57**,** 1262-1268.

Farías, T., Hajizadeh, S. and Ye, L. 2020. Cryogels with high cisplatin adsorption capacity: Towards removal of cytotoxic drugs from wastewater. *Separation and Purification Technology,* 235**,** 116203.

Feng, N., Wu, S., Song, D., Li, Y., Lu, N., Sun, L., Yu, T., Li, A. and Deng, W. 2021. Conjugated microporous polymer foams with excellent thermal insulation performance in a humid environment. *RSC Advances,* 11**,** 13957-13963.

Ferrández-Gómez, B., Ruiz-Rosas, R., Beaumont, S., Cazorla-Amorós, D. and Morallón, E. 2021. Electrochemical regeneration of spent activated carbon from drinking water treatment plant at different scale reactors. *Chemosphere,* 264**,** 128399.

Freundlich, H. 1906. Über die Adsorption in Lösungen. *Zeitschrift für Physikalische Chemie,* 57A**,** 385-470.

Gan, S., Zakaria, S., Chia, C. H. and Kaco, H. 2018. Effect of graphene oxide on thermal stability of aerogel bio-nanocomposite from cellulose-based waste biomass. *Cellulose,* 25**,** 5099-5112.

García-González, A., Zavala-Arce, R. E., Avila-Pérez, P., Rangel-Vazquez, N. A., Salazar-Rábago, J. J., García-Rivas, J. L. and García-Gaitán, B. 2021. Experimental and theoretical

study of dyes adsorption process on chitosan-based cryogel. *International Journal of Biological Macromolecules,* 169**,** 75-84.

Gogate, P. R. and Pandit, A. B. 2004. A review of imperative technologies for wastewater treatment II: hybrid methods. *Advances in Environmental Research,* 8**,** 553-597.

Groult, S., Buwalda, S. and Budtova, T. 2021. Pectin hydrogels, aerogels, cryogels and xerogels: Influence of drying on structural and release properties. *European Polymer Journal,* 149**,** 110386.

Guan, Q.-F., Yang, H.-B., Han, Z.-M., Zhou, L.-C., Zhu, Y.-B., Ling, Z.-C., Jiang, H.-B., Wang, P.-F., Ma, T., Wu, H.-A. and Yu, S.-H. 2020. Lightweight, tough, and sustainable cellulose nanofiber-derived bulk structural materials with low thermal expansion coefficient. *Science Advances,* 6**,** eaaz1114.

Gun'ko, V. M., Savina, I. N. and Mikhalovsky, S. V. 2013. Cryogels: Morphological, structural and adsorption characterisation. *Advances in Colloid and Interface Science,* 187-188**,** 1-46.

Guo, X., Shan, J., Lei, W., Ding, R., Zhang, Y. and Yang, H. 2019. Facile Synthesis of Methylsilsesquioxane Aerogels with Uniform Mesopores by Microwave Drying. *Polymers,* 11**,** 375.

Gurav, J. L., Jung, I.-K., Park, H.-H., Kang, E. S. and Nadargi, D. Y. 2010. Silica Aerogel: Synthesis and Applications. *Journal of Nanomaterials,* 2010**,** 409310.

Hajizadeh, S. 2012. *Composite Cryogels: Stationary Phase for Separation of Complex Media* Doctor of Philosophy, Lund University.

Hamaker, H. C. 1937. The London—van der Waals attraction between spherical particles. *Physica,* 4**,** 1058-1072.

Hamano, Y., Tsujimura, S., Shirai, O. and Kano, K. 2014. Control of the pore size distribution of carbon cryogels by pH adjustment of catalyst solutions. *Materials Letters,* 128**,** 191-194.

Henderson, T. M. A., Ladewig, K., Haylock, D. N., McLean, K. M. and O'Connor, A. J. 2013. Cryogels for biomedical applications. *Journal of Materials Chemistry B,* 1**,** 2682-2695.

Hernandez-Martínez, A. R., Lujan-Montelongo, J. A., Silva-Cuevas, C., Mota-Morales, J. D., Cortez-Valadez, M., Ruíz-Baltazar, Á. d. J., Cruz, M. and Herrera-Ordonez, J. 2018. Swelling and methylene blue adsorption of poly(N,N-dimethylacrylamide-co-2-hydroxyethyl methacrylate) hydrogel. *Reactive and Functional Polymers,* 122**,** 75-84.

Hokkanen, S., Repo, E., Westholm, L. J., Lou, S., Sainio, T. and Sillanpää, M. 2014. Adsorption of Ni2+, Cd2+, PO43− and NO3− from aqueous solutions by nanostructured microfibrillated cellulose modified with carbonated hydroxyapatite. *Chemical Engineering Journal,* 252**,** 64-74.

Hosseini, M., Zaki Dizaji, H., Taghavi, M. and Babaei, A. A. 2020. Preparation of ultra-lightweight and surface-tailored cellulose nanofibril composite cryogels derived from Date palm waste as powerful and low-cost heavy metals adsorbent to treat aqueous medium. *Industrial Crops and Products,* 154**,** 112696.

Hu, H. and Xu, K. 2020. Chapter 8 - Physicochemical technologies for HRPs and risk control. *In:* Ren, H.andZhang, X. (eds.) *High-Risk Pollutants in Wastewater*. Elsevier.

Hussain, A., Li, J., Wang, J., Xue, F., Chen, Y., Bin Aftab, T. and Li, D. 2018. Hybrid Monolith of Graphene/TEMPO-Oxidized Cellulose Nanofiber as Mechanically Robust, Highly Functional, and Recyclable Adsorbent of Methylene Blue Dye. *Journal of Nanomaterials,* 2018**,** 5963982.

Imaninezhad, M., Hill, L., Kolar, G., Vogt, K. and Zustiak, S. P. 2019. Templated Macroporous Polyethylene Glycol Hydrogels for Spheroid and Aggregate Cell Culture. *Bioconjugate Chemistry,* 30**,** 34-46.

Iniesta, J., Michaud, P. A., Panizza, M., Cerisola, G., Aldaz, A. and Comninellis, C. 2001. Electrochemical oxidation of phenol at boron-doped diamond electrode. *Electrochimica Acta,* 46**,** 3573-3578.

Isogai, A. 2018. Development of completely dispersed cellulose nanofibers. *Proceedings of the Japan Academy. Series B, Physical and biological sciences,* 94**,** 161-179.

Ivanov, A. E., Kozynchenko, O. P., Mikhalovska, L. I., Tennison, S. R., Jungvid, H., Gun'ko, V. M. and Mikhalovsky, S. V. 2012. Activated carbons and carbon-containing poly(vinyl alcohol) cryogels: characterization, protein adsorption and possibility of myoglobin clearance. *Physical Chemistry Chemical Physics,* 14**,** 16267-16278.

Jayanthi, S., KrishnaRao Eswar, N., Singh, S. A., Chatterjee, K., Madras, G. and Sood, A. K. 2016. Macroporous three-dimensional graphene oxide foams for dye adsorption and antibacterial applications. *RSC Advances,* 6**,** 1231-1242.

Jiang, Y., Hussain, H. and Kressler, J. 2015. Poly(vinyl alcohol) Cryogel Formation Using Biocompatible Ice Nucleating Agents. *Macromolecular Materials and Engineering,* 300**,** 181-190.

Johnson, C. 2014. 2.4 - Advances in Pretreatment and Clarification Technologies. *In:* Ahuja, S. (ed.) *Comprehensive Water Quality and Purification.* Waltham: Elsevier.

Kalijadis, A., Gavrilov, N., Jokić, B., Gilić, M., Krstić, A., Pašti, I. and Babić, B. 2020. Composition, structure and potential energy application of nitrogen doped carbon cryogels. *Materials Chemistry and Physics,* 239**,** 122120.

Kang, W., Cui, Y., Yang, Y., Guo, M., Zhao, Z., Wang, X. and Liu, X. 2021. Preparation of nitrogen-doped hollow carbon nanosphere/graphene composite aerogel for efficient removal of quinoline from wastewater. *Journal of Hazardous Materials,* 417**,** 126160.

Karimi, S., Tavakkoli Yaraki, M. and Karri, R. R. 2019. A comprehensive review of the adsorption mechanisms and factors influencing the adsorption process from the perspective of bioethanol dehydration. *Renewable and Sustainable Energy Reviews,* 107**,** 535-553.

Kemençe, N. and Bölgen, N. 2017. Gelatin- and hydroxyapatite-based cryogels for bone tissue engineering: synthesis, characterization, in vitro and in vivo biocompatibility. *Journal of Tissue Engineering and Regenerative Medicine,* 11**,** 20-33.

Khabibullin, A., Alizadehgiashi, M., Khuu, N., Prince, E., Tebbe, M. and Kumacheva, E. 2017. Injectable Shear-Thinning Fluorescent Hydrogel Formed by Cellulose Nanocrystals and Graphene Quantum Dots. *Langmuir,* 33**,** 12344-12350.

Kistler, S. S. 1931. Coherent Expanded Aerogels and Jellies. *Nature,* 127**,** 741-741.

Korhonen, J. T., Kettunen, M., Ras, R. H. A. and Ikkala, O. 2011. Hydrophobic Nanocellulose Aerogels as Floating, Sustainable, Reusable, and Recyclable Oil Absorbents. *ACS Applied Materials & Interfaces,* 3**,** 1813-1816.

Kotatha, D. and Rungrodnimitchai, S. 2018. Synthesis and Characterization of Nanofiber of Oxidized Cellulose from Nata De Coco. *International Journal of Chemical Engineering,* 2018**,** 2787035.

Kulkarni, S. and Kaware, J. 2014. Regeneration and Recovery in Adsorption- a Review. *International Journal of Innovative Science,* 1**,** 2348 – 7968.

Kumar, A. 2016. *Supermacroporous Cryogels: Biomedical and Biotechnological Applications,* Taylor & Francis Group

Kumar, A., Mishra, R., Reinwald, Y. and Bhat, S. 2010. Cryogels: Freezing unveiled by thawing. *Materials Today,* 13**,** 42-44.

Kunz Lazzari, L., Perondi, D., Zattera, A. J. and Campomanes Santana, R. M. 2021. Cellulose/Biochar Cryogels: A Study of Adsorption Kinetics and Isotherms. *Langmuir,* 37**,** 3180-3188.

Labiadh, L. and Kamali, A. R. 2019. 3D graphene nanoedges as efficient dye adsorbents with ultra-high thermal regeneration performance. *Applied Surface Science,* 490**,** 383-394.

Labiadh, L. and Kamali, A. R. 2020. Textural, structural and morphological evolution of mesoporous 3D graphene saturated with methyl orange dye during thermal regeneration. *Diamond and Related Materials,* 103**,** 107698.

Landi, E., Sciti, D., Melandri, C. and Medri, V. 2013. Ice templating of ZrB2 porous architectures. *Journal of the European Ceramic Society,* 33**,** 1599-1607.

Langmuir, I. 1918. The Adsorption of Gases on Plane Surfaces of Glass, Mica, and Platinum. *Journal of the American Chemical Society,* 40**,** 1361-1403.

Lazzari, L. K., Zampieri, V. B., Neves, R. M., Zanini, M., Zattera, A. J. and Baldasso, C. 2019. A study on adsorption isotherm and kinetics of petroleum by cellulose cryogels. *Cellulose,* 26**,** 1231-1246.

Lazzari, L. K., Zampieri, V. B., Zanini, M., Zattera, A. J. and Baldasso, C. 2017. Sorption capacity of hydrophobic cellulose cryogels silanized by two different methods. *Cellulose,* 24**,** 3421-3431.

Li, S.-S., Song, Y.-L., Yang, H.-R., An, Q.-D., Xiao, Z.-Y. and Zhai, S.-R. 2020. Carboxymethyl cellulose-based cryogels for efficient heavy metal capture: Aluminum-mediated assembly

process and sorption mechanism. *International Journal of Biological Macromolecules,* 164**,** 3275-3286.

Li, Y., Fu, Z.-Y. and Su, B.-L. 2012. Hierarchically Structured Porous Materials for Energy Conversion and Storage. *Advanced Functional Materials,* 22**,** 4634-4667.

Li, Z., Yang, L., Cao, H., Chang, Y., Tang, K., Cao, Z., Chang, J., Cao, Y., Wang, W., Gao, M., Liu, C., Liu, D., Zhao, H., Zhang, Y. and Li, M. 2017. Carbon materials derived from chitosan/cellulose cryogel-supported zeolite imidazole frameworks for potential supercapacitor application. *Carbohydrate Polymers,* 175**,** 223-230.

Liao, H.-T., Shalumon, K. T., Chang, K.-H., Sheu, C. and Chen, J.-P. 2016. Investigation of synergistic effects of inductive and conductive factors in gelatin-based cryogels for bone tissue engineering. *Journal of Materials Chemistry B,* 4**,** 1827-1841.

Lipp, G. and Körber, C. 1993. On the engulfment of spherical particles by a moving ice-liquid interface. *Journal of Crystal Growth,* 130**,** 475-489.

Liu, K., Du, H., Zheng, T., Liu, H., Zhang, M., Zhang, R., Li, H., Xie, H., Zhang, X., Ma, M. and Si, C. 2021a. Recent advances in cellulose and its derivatives for oilfield applications. *Carbohydrate Polymers,* 259**,** 117740.

Liu, L., Xie, J. P., Li, Y. J., Zhang, Q. and Yao, J. M. 2016. Three-dimensional macroporous cellulose-based bioadsorbents for efficient removal of nickel ions from aqueous solution. *Cellulose,* 23**,** 723-736.

Liu, M., Liu, H., Bai, L., Liu, Y., Cheng, J. and Yang, G. 2011. Temperature swing adsorption of melamine on thermosensitive poly(N-isopropylacrylamide) cryogels. *Journal of Materials Science,* 46**,** 4820-4825.

Liu, S., Xiao, J., Chen, K., Xiao, W. and Li, B. 2021b. [The research advances of three dimensional porous cryogel for tissue engineering]. *Sheng wu yi xue gong cheng xue za zhi = Journal of biomedical engineering = Shengwu yixue gongchengxue zazhi,* 38**,** 393-398.

Lofrano, G., Meriç, S., Zengin, G. E. and Orhon, D. 2013. Chemical and biological treatment technologies for leather tannery chemicals and wastewaters: A review. *Science of The Total Environment,* 461-462**,** 265-281.

Lopez Pablos, M. F. 2021. *Synthesis of Graphene for Wastewater Treatment by Adsorption and Electrochemical Regeneration.* University of Calgary

Lozinsky, V. I., Galaev, I. Y., Plieva, F. M., Savina, I. N., Jungvid, H. and Mattiasson, B. 2003. Polymeric cryogels as promising materials of biotechnological interest. *Trends in Biotechnology,* 21**,** 445-451.

Lozinsky, V. I. and Plieva, F. M. 1998. Poly(vinyl alcohol) cryogels employed as matrices for cell immobilization. 3. Overview of recent research and developments. *Enzyme and Microbial Technology,* 23**,** 227-242.

Lv, G., Wu, D. and Fu, R. 2009. Performance of carbon aerogels particle electrodes for the aqueous phase electro-catalytic oxidation of simulated phenol wastewaters. *Journal of Hazardous Materials,* 165**,** 961-966.

Ma, D., Yi, H., Lai, C., Liu, X., Huo, X., An, Z., Li, L., Fu, Y., Li, B., Zhang, M., Qin, L., Liu, S. and Yang, L. 2021. Critical review of advanced oxidation processes in organic wastewater treatment. *Chemosphere,* 275**,** 130104.

Marcuz, C., Alves Mourão, C., Haupt, K. and Alves Bueno, S. M. 2021. Performance of phospho-L-tyrosine immobilized onto alginate/polyacrylamide-based cryogels: Effect of ligand

coupling on human IgG adsorption and Fab fragments separation. *Journal of Chromatography B,* 1165**,** 122530.

Martínez-Huitle, C. A. and Ferro, S. 2006. Electrochemical oxidation of organic pollutants for the wastewater treatment: direct and indirect processes. *Chemical Society Reviews,* 35**,** 1324-1340.

McQuillan, R. V. 2021. *The electrochemical regeneration of granular activated carbons in situ of permeable reactive barriers.* The University of Melbourne.

Memic, A., Colombani, T., Eggermont, L. J., Rezaeeyazdi, M., Steingold, J., Rogers, Z. J., Navare, K. J., Mohammed, H. S. and Bencherif, S. A. 2019. Latest Advances in Cryogel Technology for Biomedical Applications. *Advanced Therapeutics,* 2**,** 1800114.

Mendoza, L., Batchelor, W., Tabor, R. F. and Garnier, G. 2018. Gelation mechanism of cellulose nanofibre gels: A colloids and interfacial perspective. *Journal of Colloid and Interface Science,* 509**,** 39-46.

Milakin, K. A., Gavrilov, N., Pašti, I. A., Trchová, M., Zasońska, B. A., Stejskal, J. and Bober, P. 2020. Carbon Materials Derived from Poly(aniline-co-p-phenylenediamine) Cryogels. *Polymers,* 12**,** 11.

Mohamed, M. G., Ahmed, M. M. M., Du, W.-T. and Kuo, S.-W. 2021. Meso/Microporous Carbons from Conjugated Hyper-Crosslinked Polymers Based on Tetraphenylethene for High-Performance CO2 Capture and Supercapacitor. *Molecules,* 26**,** 738.

Moosavi, S., Gan, S., Chia, C. H. and Zakaria, S. 2020. Evaluation of Crosslinking Effect on Thermo-mechanical, Acoustic Insulation and Water Absorption Performance of Biomass-Derived Cellulose Cryogels. *Journal of Polymers and the Environment,* 28**,** 1180-1189.

Mourabet, M., El Boujaady, H., El Rhilassi, A., Ramdane, H., Bennani-Ziatni, M., El Hamri, R. and Taitai, A. 2011. Defluoridation of water using Brushite: Equilibrium, kinetic and thermodynamic studies. *Desalination,* 278**,** 1-9.

Mukai, S. R., Nishihara, H. and Tamon, H. 2008. Morphology maps of ice-templated silica gels derived from silica hydrogels and hydrosols. *Microporous and Mesoporous Materials,* 116**,** 166-170.

Musa, M. A. and Idrus, S. 2021. Physical and Biological Treatment Technologies of Slaughterhouse Wastewater: A Review. *Sustainability,* 13**,** 4656.

Mustafa, R. and Asmatulu, E. 2020. Preparation of activated carbon using fruit, paper and clothing wastes for wastewater treatment. *Journal of Water Process Engineering,* 35**,** 101239.

Nagpal, M. and Kakkar, R. 2019. Use of metal oxides for the adsorptive removal of toxic organic pollutants. *Separation and Purification Technology,* 211**,** 522-539.

Narbaitz, R. M. and McEwen, J. 2012. Electrochemical regeneration of field spent GAC from two water treatment plants. *Water Res,* 46**,** 4852-60.

Nkrumah-Amoako, K., Roberts, E. P. L., Brown, N. W. and Holmes, S. M. 2014. The effects of anodic treatment on the surface chemistry of a Graphite Intercalation Compound. *Electrochimica Acta,* 135**,** 568-577.

Oelschlaeger, C., Bossler, F. and Willenbacher, N. 2016. Synthesis, Structural and Micromechanical Properties of 3D Hyaluronic Acid-Based Cryogel Scaffolds. *Biomacromolecules,* 17**,** 580-589.

Okay, O. 2014. *Polymeric Cryogels: Macroporous Gels with Remarkable Properties*, Springer, Cham.

Omorogie, M. O., Babalola, J. O. and Unuabonah, E. I. 2016. Regeneration strategies for spent solid matrices used in adsorption of organic pollutants from surface water: a critical review. *Desalination and Water Treatment,* 57**,** 518-544.

Pajonk, G. M., Repellin-Lacroix, M., Abouarnadasse, S., Chaouki, J. and Klavana, D. 1990. From sol-gel to aerogels and cryogels. *Journal of Non-Crystalline Solids,* 121**,** 66-67.

Pan, M., Shan, C., Zhang, X., Zhang, Y., Zhu, C., Gao, G. and Pan, B. 2018a. Environmentally Friendly in Situ Regeneration of Graphene Aerogel as a Model Conductive Adsorbent. *Environmental Science & Technology,* 52**,** 739-746.

Pan, Z.-Z., Govedarica, A., Nishihara, H., Tang, R., Wang, C., Luo, Y., Lv, W., Kang, F.-Y., Trifkovic, M. and Yang, Q.-H. 2021. pH-Dependent Morphology Control of Cellulose Nanofiber/Graphene Oxide Cryogels. *Small,* 17**,** 2005564.

Pan, Z.-Z., Lv, W., He, Y.-B., Zhao, Y., Zhou, G., Dong, L., Niu, S., Zhang, C., Lyu, R., Wang, C., Shi, H., Zhang, W., Kang, F., Nishihara, H. and Yang, Q.-H. 2018b. A Nacre-Like Carbon Nanotube Sheet for High Performance Li-Polysulfide Batteries with High Sulfur Loading. *Advanced Science,* 5.

Pan, Z.-Z., Nishihara, H., Iwamura, S., Sekiguchi, T., Sato, A., Isogai, A., Kang, F., Kyotani, T. and Yang, Q.-H. 2016. Cellulose Nanofiber as a Distinct Structure-Directing Agent for Xylem-like Microhoneycomb Monoliths by Unidirectional Freeze-Drying. *ACS Nano,* 10**,** 10689-10697.

Panizza, M., Barbucci, A., Ricotti, R. and Cerisola, G. 2007. Electrochemical degradation of methylene blue. *Separation and Purification Technology,* 54**,** 382-387.

Pazos, V., Mongrain, R. and Tardif, J. C. 2009. Polyvinyl alcohol cryogel: Optimizing the parameters of cryogenic treatment using hyperelastic models. *Journal of the Mechanical Behavior of Biomedical Materials,* 2**,** 542-549.

Petrov, P., Petrova, E., Stamenova, R., Tsvetanov, C. B. and Riess, G. 2006. Cryogels of cellulose derivatives prepared via UV irradiation of moderately frozen systems. *Polymer,* 47**,** 6481-6484.

Pierpaoli, M., Jakobczyk, P., Sawczak, M., Łuczkiewicz, A., Fudala-Książek, S. and Bogdanowicz, R. 2021. Carbon nanoarchitectures as high-performance electrodes for the electrochemical oxidation of landfill leachate. *Journal of Hazardous Materials,* 401**,** 123407.

Pietrzyk, D. J. and Frank, C. W. 1979. Chapter Twenty-Three - Column Methods. *In:* Pietrzyk, D. J.andFrank, C. W. (eds.) *Analytical Chemistry.* Academic Press.

Plieva, F. M., Galaev, I. Y., Noppe, W. and Mattiasson, B. 2008. Cryogel applications in microbiology. *Trends in Microbiology,* 16**,** 543-551.

Pons, A., Casas, L., Estop, E., Molins, E., Harris, K. D. M. and Xu, M. 2012. A new route to aerogels: Monolithic silica cryogels. *Journal of Non-Crystalline Solids,* 358**,** 461-469.

Porter, M. M., Imperio, R., Wen, M., Meyers, M. A. and McKittrick, J. 2014. Bioinspired Scaffolds with Varying Pore Architectures and Mechanical Properties. *Advanced Functional Materials,* 24**,** 1978-1987.

Qu, J. 2008. Research progress of novel adsorption processes in water purification: A review. *Journal of Environmental Sciences,* 20**,** 1-13.

Rahmatika, A. M., Goi, Y., Kitamura, T., Widiyastuti, W. and Ogi, T. 2019. TEMPO-oxidized cellulose nanofiber (TOCN) decorated macroporous silica particles: Synthesis,

characterization, and their application in protein adsorption. *Materials Science and Engineering: C,* 105**,** 110033.

Rai, A. K. 2020. pH-responsive Pickering emulsion using magnetic nanoparticles.

Ramaswamy, S., Huang, H. J. and Ramarao, B. V. 2013. *Separation and Purification Technologies in Biorefineries*, John Wiley and Sons.

Ramirez, N., Zámbó, D., Sardella, F., Kißling, P. A., Schlosser, A., Graf, R. T., Pluta, D., Deiana, C. and Bigall, N. C. 2021. Pd-Doped Cellulose Carbon Aerogels for Energy Storage Applications. *Advanced Materials Interfaces,* 8**,** 2100310.

Rashid, R., Shafiq, I., Akhter, P., Iqbal, M. J. and Hussain, M. 2021. A state-of-the-art review on wastewater treatment techniques: the effectiveness of adsorption method. *Environmental Science and Pollution Research,* 28**,** 9050-9066.

Rattanakunsong, N. and Bunkoed, O. 2020. A porous composite monolith sorbent of polyaniline, multiwall carbon nanotubes and chitosan cryogel for aromatic compounds extraction. *Microchemical Journal,* 154**,** 104562.

Razavi, M., Qiao, Y. and Thakor, A. S. 2019. Three-dimensional cryogels for biomedical applications. *Journal of Biomedical Materials Research Part A,* 107**,** 2736-2755.

Reddy, R. M., Srivastava, A. and Kumar, A. 2013. Monosaccharide-Responsive Phenylboronate-Polyol Cell Scaffolds for Cell Sheet and Tissue Engineering Applications. *PLOS ONE,* 8**,** e77861.

Renu, Agarwal, M. and Singh, K. 2016. Heavy metal removal from wastewater using various adsorbents: a review. *Journal of Water Reuse and Desalination,* 7**,** 387-419.

Sabzehmeidani, M. M., Mahnaee, S., Ghaedi, M., Heidari, H. and Roy, V. A. L. 2021. Carbon based materials: a review of adsorbents for inorganic and organic compounds. *Materials Advances,* 2**,** 598-627.

Saito, T. and Isogai, A. 2004. TEMPO-Mediated Oxidation of Native Cellulose. The Effect of Oxidation Conditions on Chemical and Crystal Structures of the Water-Insoluble Fractions. *Biomacromolecules,* 5**,** 1983-1989.

Saito, T., Kimura, S., Nishiyama, Y. and Isogai, A. 2007. Cellulose Nanofibers Prepared by TEMPO-Mediated Oxidation of Native Cellulose. *Biomacromolecules,* 8**,** 2485-2491.

Saito, T., Nishiyama, Y., Putaux, J.-L., Vignon, M. and Isogai, A. 2006. Homogeneous Suspensions of Individualized Microfibrils from TEMPO-Catalyzed Oxidation of Native Cellulose. *Biomacromolecules,* 7**,** 1687-1691.

Samarghandi, M. R., Dargahi, A., Shabanloo, A., Nasab, H. Z., Vaziri, Y. and Ansari, A. 2020. Electrochemical degradation of methylene blue dye using a graphite doped PbO2 anode: Optimization of operational parameters, degradation pathway and improving the biodegradability of textile wastewater. *Arabian Journal of Chemistry,* 13**,** 6847-6864.

Samer, M. 2015. Biological and Chemical Wastewater Treatment Processes, Wastewater Treatment Engineering. IntechOpen.

Savina, I. N., Ingavle, G. C., Cundy, A. B. and Mikhalovsky, S. V. 2016. A simple method for the production of large volume 3D macroporous hydrogels for advanced biotechnological, medical and environmental applications. *Scientific Reports,* 6**,** 21154.

Saylan, Y. and Denizli, A. 2019. Supermacroporous Composite Cryogels in Biomedical Applications. *Gels,* 5**,** 20.

Schvezov, C. E. and Weinberg, F. 1985. Interaction of iron particles with a solid-liquid interface in lead and lead alloys. *Metallurgical Transactions B,* 16**,** 367-375.

Scialdone, O., Randazzo, S., Galia, A. and Silvestri, G. 2009. Electrochemical oxidation of organics in water: Role of operative parameters in the absence and in the presence of NaCl. *Water Research,* 43**,** 2260-2272.

Seddiqi, H., Oliaei, E., Honarkar, H., Jin, J., Geonzon, L. C., Bacabac, R. G. and Klein-Nulend, J. 2021. Cellulose and its derivatives: towards biomedical applications. *Cellulose,* 28**,** 1893-1931.

Sharif, F., Gagnon, L. R., Mulmi, S. and Roberts, E. P. L. 2017. Electrochemical regeneration of a reduced graphene oxide/magnetite composite adsorbent loaded with methylene blue. *Water Research,* 114**,** 237-245.

Sharif, F. and Roberts, E. P. L. 2020. Electrochemical Oxidation of an Organic Dye Adsorbed on Tin Oxide and Antimony Doped Tin Oxide Graphene Composites. *Catalysts,* 10**,** 263.

Sharif, F., Zeraati, A. S., Ganjeh-Anzabi, P., Yasri, N., Perez-Page, M., Holmes, S. M., Sundararaj, U., Trifkovic, M. and Roberts, E. P. L. 2020. Synthesis of a high-temperature stable electrochemically exfoliated graphene. *Carbon,* 157**,** 681-692.

Sheintuch, M. and Matatov-Meytal, Y. I. 1999. Comparison of catalytic processes with other regeneration methods of activated carbon. *Catalysis Today,* 53**,** 73-80.

Shlyakhtin, O. A. and Oh, Y.-J. 2008. Inorganic cryogels for energy saving and conversion. *Journal of Electroceramics,* 23**,** 452.

Soni, B., Hassan, E. B. and Mahmoud, B. 2015. Chemical isolation and characterization of different cellulose nanofibers from cotton stalks. *Carbohydrate Polymers,* 134**,** 581-589.

Sparks, D. L. 2003. 5 - Sorption Phenomena on Soils. *In:* Sparks, D. L. (ed.) *Environmental Soil Chemistry (Second Edition).* Burlington: Academic Press.

Su, L. F., Miao, L., Tanemura, S. and Xu, G. 2012. Low-cost and fast synthesis of nanoporous silica cryogels for thermal insulation applications. *Science and Technology of Advanced Materials,* 13**,** 035003.

Sun, X., Yang, L., Li, Q., Zhao, J., Li, X., Wang, X. and Liu, H. 2014. Amino-functionalized magnetic cellulose nanocomposite as adsorbent for removal of Cr(VI): Synthesis and adsorption studies. *Chemical Engineering Journal,* 241**,** 175-183.

Tamon, H., Ishizaka, H., Yamamoto, T. and Suzuki, T. 2001. FREEZE DRYING FOR PREPARATION OF AEROGEL-LIKE CARBON. *Drying Technology,* 19**,** 313-324.

Tang, L., Feng, Y., He, W. and Yang, F. 2019. Combination of graphene oxide with flax-derived cellulose dissolved in NaOH/urea medium to generate hierarchically structured composite carbon aerogels. *Industrial Crops and Products,* 130**,** 179-183.

Tang, Y., Qiu, S., Wu, C., Miao, Q. and Zhao, K. 2016. Freeze cast fabrication of porous ceramics using tert-butyl alcohol–water crystals as template. *Journal of the European Ceramic Society,* 36**,** 1513-1518.

Toledo, P. V. O., Martins, B. F., Pirich, C. L., Sierakowski, M. R., Neto, E. T. and Petri, D. F. S. 2019. Cellulose Based Cryogels as Adsorbents for Organic Pollutants. *Macromolecular Symposia,* 383**,** 1800013.

Tyshkunova, I. V., Chukhchin, D. G., Gofman, I. V., Poshina, D. N. and Skorik, Y. A. 2021. Cellulose cryogels prepared by regeneration from phosphoric acid solutions. *Cellulose,* 28**,** 4975-4989.

Vargas, R., Borrás, C., Méndez, D., Mostany, J. and Scharifker, B. R. 2016. Electrochemical oxygen transfer reactions: electrode materials, surface processes, kinetic models, linear free energy correlations, and perspectives. *Journal of Solid State Electrochemistry,* 20**,** 875-893.

Wales, D. J., Grand, J., Ting, V. P., Burke, R. D., Edler, K. J., Bowen, C. R., Mintova, S. and Burrows, A. D. 2015. Gas sensing using porous materials for automotive applications. *Chemical Society Reviews,* 44**,** 4290-4321.

Wang, D.-C., Yu, H.-Y., Song, M.-L., Yang, R.-T. and Yao, J.-M. 2017. Superfast Adsorption–Disinfection Cryogels Decorated with Cellulose Nanocrystal/Zinc Oxide Nanorod Clusters for Water-Purifying Microdevices. *ACS Sustainable Chemistry & Engineering,* 5**,** 6776-6785.

Wang, L. and Balasubramanian, N. 2009. Electrochemical regeneration of granular activated carbon saturated with organic compounds. *Chemical Engineering Journal,* 155**,** 763-768.

Wegst, U. G. K., Schecter, M., Donius, A. E. and Hunger, P. M. 2010. Biomaterials by freeze casting. *Philosophical Transactions of the Royal Society A: Mathematical, Physical and Engineering Sciences,* 368**,** 2099-2121.

Worch, E. 2012. *Adsorption technology in water treatment: fundamentals, processes, and modeling.*, DE GRUYTER.

Wu, L., Li, Y., Fu, Z. and Su, B.-L. 2020. Hierarchically structured porous materials: synthesis strategies and applications in energy storage. *National Science Review,* 7**,** 1667-1701.

Wu, X., Song, X., Chen, H. and Yu, J. 2021. Experimental study and quantum chemical calculation of free radical reactions in p-nitrophenol degradation during electrochemical oxidation process. *Journal of Water Process Engineering,* 40**,** 101769.

Yahya, N., Aziz, F., Jamaludin, N. A., A. Mutalib, M., Ismail, A. F., W. Salleh, W. N., Jaafar, J., Yusof, N. and A. Ludin, N. 2018. A review of integrated photocatalyst adsorbents for wastewater treatment. *Journal of Environmental Chemical Engineering,* 6**,** 7411-7425.

Yang, K., Peng, H., Wen, Y. and Li, N. 2010. Re-examination of characteristic FTIR spectrum of secondary layer in bilayer oleic acid-coated Fe3O4 nanoparticles. *Applied Surface Science,* 256**,** 3093-3097.

Yang, X., Debeli, D. K., Shan, G. and Pan, P. 2020. Selective adsorption and high recovery of La3+ using graphene oxide/poly (N-isopropyl acrylamide-maleic acid) cryogel. *Chemical Engineering Journal,* 379**,** 122335.

Yao, L., Lu, Y., Wang, Y. and Hu, L. 2014. Effect of graphene oxide on the solution rheology and the film structure and properties of cellulose carbamate. *Carbon,* 69**,** 552-562.

Yao, W., Jiang, X., Li, M., Li, Y., Liu, Y., Zhan, X., Fu, G. and Tang, Y. 2021. Engineering hollow porous platinum-silver double-shelled nanocages for efficient electro-oxidation of methanol. *Applied Catalysis B: Environmental,* 282**,** 119595.

Yi, F., Chen, S. and Yuan, C. e. 2008. Effect of activated carbon fiber anode structure and electrolysis conditions on electrochemical degradation of dye wastewater. *Journal of Hazardous Materials,* 157**,** 79-87.

Yin, M., Li, X., Liu, Y. and Ren, X. 2021. Functional chitosan/glycidyl methacrylate-based cryogels for efficient removal of cationic and anionic dyes and antibacterial applications. *Carbohydrate Polymers,* 266**,** 118129.

Yoon, J. I., Choi, K. S. and Chang, S. P. 2017. A novel means of fabricating microporous structures for the dielectric layers of capacitive pressure sensor. *Microelectronic Engineering,* 179**,** 60-66.

Yousefi, N., Lu, X., Elimelech, M. and Tufenkji, N. 2019. Environmental performance of graphene-based 3D macrostructures. *Nature Nanotechnology,* 14**,** 107-119.

Yu, L., Xue, J., Zhang, L., Tang, C. and Guo, Y. 2021. Fabrication of a stable Ti/Pb-TiOxNWs/PbO2 anode and its application in benzoquinone degradation. *Electrochimica Acta,* 368**,** 137532.

Zhang, J. X. J. and Hoshino, K. 2019. Chapter 7 - Nanomaterials for molecular sensing. *In:* Zhang, J. X. J.andHoshino, K. (eds.) *Molecular Sensors and Nanodevices (Second Edition).* Academic Press.

Zhang, K., Barhoum, A., Xiaoqing, C., Li, H. and Samyn, P. 2019. *Cellulose Nanofibers: Fabrication and Surface Functionalization Techniques*, Springer, Cham.

Zhang, L., Peng, Y., Zhang, J., Chen, L., Meng, X. and Xiao, F.-S. 2016. Adsorptive and catalytic properties in the removal of volatile organic compounds over zeolite-based materials. *Chinese Journal of Catalysis,* 37**,** 800-809.

Zhang, Y., Yu, S., Lou, G., Shen, Y., Chen, H., Shen, Z., Zhao, S., Zhang, J., Chai, S. and Zou, Q. 2017. Review of macroporous materials as electrochemical supercapacitor electrodes. *Journal of Materials Science,* 52**,** 11201-11228.

Zhang, Y., Zhou, K., Bao, Y. and Zhang, D. 2013. Effects of rheological properties on ice-templated porous hydroxyapatite ceramics. *Materials Science and Engineering: C,* 33**,** 340-346.

Zhong, T., Feng, X., Sun, L., Zhang, J., Tian, Y. and Zhang, X. 2020. Highly effective adsorption of copper ions by poly(vinyl imidazole) cryogels. *Polymer Bulletin*.

Zhou, W., Meng, X., Gao, J., Zhao, H., Zhao, G. and Ma, J. 2021. Electrochemical regeneration of carbon-based adsorbents: a review of regeneration mechanisms, reactors, and future prospects. *Chemical Engineering Journal Advances,* 5**,** 100083.

Zhou, Y., Zhang, M., Hu, X., Wang, X., Niu, J. and Ma, T. 2013. Adsorption of Cationic Dyes on a Cellulose-Based Multicarboxyl Adsorbent. *Journal of Chemical & Engineering Data,* 58**,** 413-421.

Zhu, L., Shen, D. and Luo, K. H. 2020. A critical review on VOCs adsorption by different porous materials: Species, mechanisms and modification methods. *Journal of Hazardous Materials,* 389**,** 122102.

Zhu, X., Hu, W., Feng, C., Chen, N., Chen, H., Kuang, P., Deng, Y. and Ma, L. 2021. Electrochemical oxidation of aniline using Ti/RuO2-SnO2 and Ti/RuO2-IrO2 as anode. *Chemosphere,* 269**,** 128734.

Zou, F. and Budtova, T. 2021. Tailoring the morphology and properties of starch aerogels and cryogels via starch source and process parameter. *Carbohydrate Polymers,* 255**,** 117344.

CCC RightsLink®

Home | Help | Email Support | SAQR ABUHATAB

Cryogels: Freezing unveiled by thawing

Author: Ashok Kumar,Ruchi Mishra,Yvonne Reinwald,Sumrita Bhat
Publication: Materials Today
Publisher: Elsevier
Date: November 2010

Order Completed

Thank you for your order.

This Agreement between Mr. SAQR ABUHATAB ("You") and Elsevier ("Elsevier") consists of your license details and the terms and conditions provided by Elsevier and Copyright Clearance Center.

Your confirmation email will contain your order number for future reference.

License Number	5217000280795
License date	Dec 27, 2021

Printable Details

Licensed Content

Licensed Content Publisher	Elsevier
Licensed Content Publication	Materials Today
Licensed Content Title	Cryogels: Freezing unveiled by thawing
Licensed Content Author	Ashok Kumar,Ruchi Mishra,Yvonne Reinwald,Sumrita Bhat
Licensed Content Date	Nov 1, 2010
Licensed Content Volume	13
Licensed Content Issue	11
Licensed Content Pages	3

Order Details

Type of Use	reuse in a thesis/dissertation
Portion	figures/tables/illustrations
Number of figures/tables /illustrations	1
Format	both print and electronic
Are you the author of this Elsevier article?	No
Will you be translating?	No

CCC RightsLink®

Home | Help | Email Support | SAQR ABUHATAB

Effect of graphene oxide on the solution rheology and the film structure and properties of cellulose carbamate

Author: Lili Yao,Yonggen Lu,Yibo Wang,Leiyang Hu
Publication: Carbon
Publisher: Elsevier
Date: April 2014

Order Completed

Thank you for your order.

This Agreement between Mr. SAQR ABUHATAB ("You") and Elsevier ("Elsevier") consists of your license details and the terms and conditions provided by Elsevier and Copyright Clearance Center.

Your confirmation email will contain your order number for future reference.

License Number	5217030106465
License date	Dec 27, 2021

Printable Details

Licensed Content

Licensed Content Publisher	Elsevier
Licensed Content Publication	Carbon
Licensed Content Title	Effect of graphene oxide on the solution rheology and the film structure and properties of cellulose carbamate
Licensed Content Author	Lili Yao,Yonggen Lu,Yibo Wang,Leiyang Hu
Licensed Content Date	Apr 1, 2014
Licensed Content Volume	69
Licensed Content Issue	n/a
Licensed Content Pages	11

Order Details

Type of Use	reuse in a thesis/dissertation
Portion	figures/tables/illustrations
Number of figures/tables /illustrations	1
Format	both print and electronic
Are you the author of this Elsevier article?	No
Will you be translating?	No

CCC RightsLink®

Home | Help | Email Support | SAQR ABUHATAB

pH-Dependent Morphology Control of Cellulose Nanofiber/Graphene Oxide Cryogels

Author: Zheng-Ze Pan, Aleksandra Govedarica, Hirotomo Nishihara, et al
Publication: Small
Publisher: John Wiley and Sons
Date: Dec 22, 2020

Order Completed

Thank you for your order.

This Agreement between Mr. SAQR ABUHATAB ("You") and John Wiley and Sons ("John Wiley and Sons") consists of your license details and the terms and conditions provided by John Wiley and Sons and Copyright Clearance Center.

Your confirmation email will contain your order number for future reference.

License Number	5217000539310
License date	Dec 27, 2021

Printable Details

Licensed Content

Licensed Content Publisher	John Wiley and Sons
Licensed Content Publication	Small
Licensed Content Title	pH-Dependent Morphology Control of Cellulose Nanofiber/Graphene Oxide Cryogels
Licensed Content Author	Zheng-Ze Pan, Aleksandra Govedarica, Hirotomo Nishihara, et al
Licensed Content Date	Dec 22, 2020
Licensed Content Volume	17
Licensed Content Issue	3
Licensed Content Pages	8

Order Details

Type of use	Dissertation/Thesis
Requestor type	University/Academic
Format	Print and electronic
Portion	Figure/table
Number of figures/tables	1
Will you be translating?	No

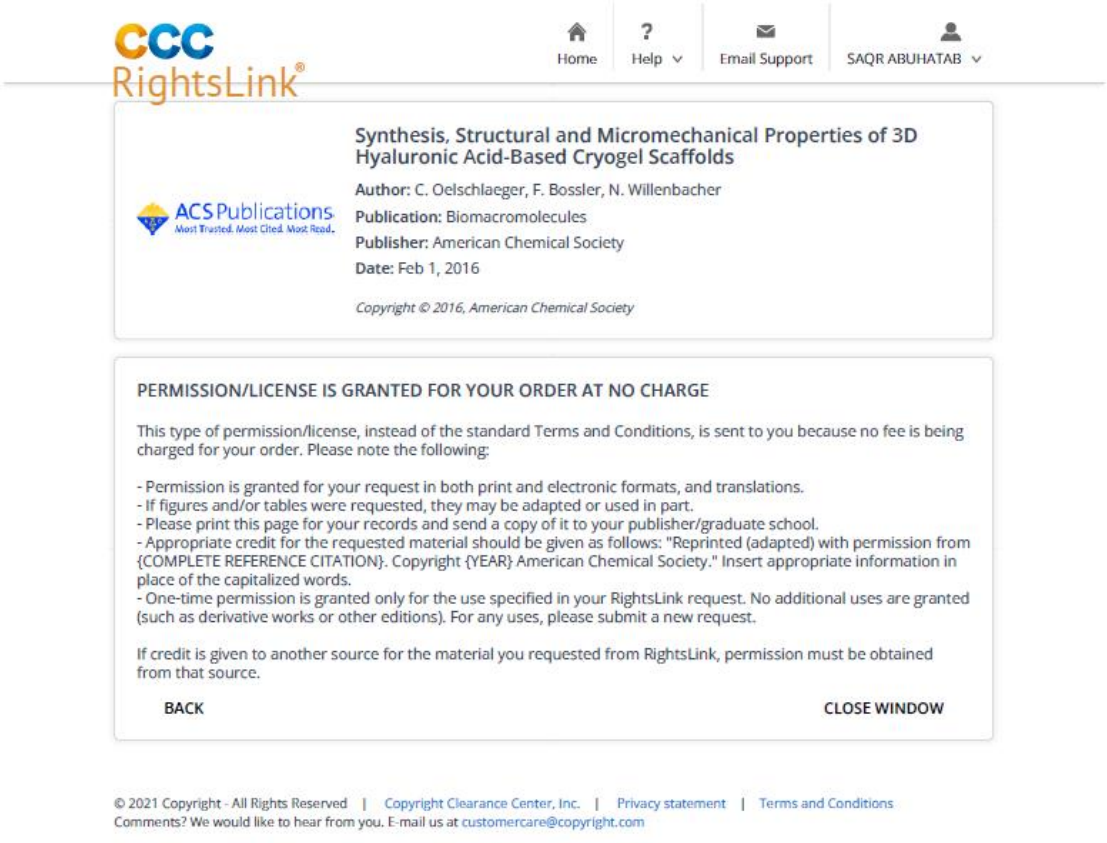

RightsLink

Home | Help | Email Support | SAQR ABUHATAB

ACS Publications
Most Trusted. Most Cited. Most Read.

Synthesis, Structural and Micromechanical Properties of 3D Hyaluronic Acid-Based Cryogel Scaffolds

Author: C. Oelschlaeger, F. Bossler, N. Willenbacher

Publication: Biomacromolecules

Publisher: American Chemical Society

Date: Feb 1, 2016

Copyright © 2016, American Chemical Society

PERMISSION/LICENSE IS GRANTED FOR YOUR ORDER AT NO CHARGE

This type of permission/license, instead of the standard Terms and Conditions, is sent to you because no fee is being charged for your order. Please note the following:

- Permission is granted for your request in both print and electronic formats, and translations.
- If figures and/or tables were requested, they may be adapted or used in part.
- Please print this page for your records and send a copy of it to your publisher/graduate school.
- Appropriate credit for the requested material should be given as follows: "Reprinted (adapted) with permission from {COMPLETE REFERENCE CITATION}. Copyright {YEAR} American Chemical Society." Insert appropriate information in place of the capitalized words.
- One-time permission is granted only for the use specified in your RightsLink request. No additional uses are granted (such as derivative works or other editions). For any uses, please submit a new request.

If credit is given to another source for the material you requested from RightsLink, permission must be obtained from that source.

BACK CLOSE WINDOW

CCC RightsLink®

Home | Help | Email Support | SAQR ABUHATAB

Contributions of electrochemical oxidation to waste-water treatment: fundamentals and review of applications

Author: Inmaculada Ortiz, Ane Urtiaga, Ángela Anglada
Publication: Journal of Chemical Technology & Biotechnology
Publisher: John Wiley and Sons
Date: May 28, 2009

Order Completed

Thank you for your order.

This Agreement between Mr. SAQR ABUHATAB ("You") and John Wiley and Sons ("John Wiley and Sons") consists of your license details and the terms and conditions provided by John Wiley and Sons and Copyright Clearance Center.

Your confirmation email will contain your order number for future reference.

License Number	5217021252085
License date	Dec 27, 2021

Printable Details

Licensed Content

Licensed Content Publisher	John Wiley and Sons
Licensed Content Publication	Journal of Chemical Technology & Biotechnology
Licensed Content Title	Contributions of electrochemical oxidation to waste-water treatment: fundamentals and review of applications
Licensed Content Author	Inmaculada Ortiz, Ane Urtiaga, Ángela Anglada
Licensed Content Date	May 28, 2009
Licensed Content Volume	84
Licensed Content Issue	12
Licensed Content Pages	9

Order Details

Type of use	Dissertation/Thesis
Requestor type	University/Academic
Format	Print and electronic
Portion	Figure/table
Number of figures/tables	1
Will you be translating?	No